



## Article

# Establishing Provenance from Highly Impoverished Heavy Mineral Suites: Detrital Apatite and Zircon Geochronology of Central North Sea Triassic Sandstones

Iain P. Greig<sup>1,2,\*</sup>, Andrew Morton<sup>1,3,\*</sup>, Dirk Frei<sup>4</sup>  and Adrian Hartley<sup>1</sup> <sup>1</sup> Department of Geology and Geophysics, University of Aberdeen, Aberdeen AB24 3UE, UK<sup>2</sup> Clachan Geoscience, 6 Hopcroft Terrace, Aberdeen AB21 9RL, UK<sup>3</sup> CASP, West Building, Madingley Road, Cambridge CB3 0UD, UK<sup>4</sup> Department of Earth Sciences, University of the Western Cape, Bellville 7530, South Africa

\* Correspondence: iain.hmresearch@gmail.com (I.P.G.); heavyminerals@hotmail.com (A.M.)

**Abstract:** A study of Triassic sandstones in the central North Sea, UK, has shown that combined detrital zircon and apatite geochronology and apatite trace element analysis is a powerful tool for reconstructing provenance for sandstones with diagenetically impoverished heavy mineral suites. Sandstones in the earlier part of the succession (Bunter Sandstone Member and Judy Sandstone Member) have characteristics that indicate derivation from Moinian–Dalradian metasediments affected by Caledonian tectonothermal events, in conjunction with a Palaeoproterozoic–Archaean source unaffected by Caledonian metamorphism. Palaeogeographic reconstructions indicate that the sediment cannot have been input directly from either of these cratonic areas. This, in conjunction with the presence of common rounded apatite, indicates that recycling is the most likely possibility. The zircon-apatite association in the younger Joanne Sandstone Member sandstones indicates derivation from lithologies with mid-Proterozoic zircons (either crystalline basement or metasediments in the Caledonian Nappes), subjected to Caledonian metamorphism to generate early Palaeozoic apatites. This combination is compatible with a source region in southern and western Norway. The low degree of textural maturity associated with the detrital apatite, together with the unimodal Caledonian age grouping, indicates the Joanne sandstones have a strong first-cycle component.

**Keywords:** central North Sea; Triassic; Skagerrak; provenance; zircon U-Pb; apatite U-Pb



**Citation:** Greig, I.P.; Morton, A.; Frei, D.; Hartley, A. Establishing Provenance from Highly Impoverished Heavy Mineral Suites: Detrital Apatite and Zircon Geochronology of Central North Sea Triassic Sandstones. *Geosciences* **2023**, *13*, 13. <https://doi.org/10.3390/geosciences13010013>

Academic Editors: Henrik Drake and Jesus Martinez-Frias

Received: 8 November 2022

Revised: 20 December 2022

Accepted: 25 December 2022

Published: 30 December 2022



**Copyright:** © 2022 by the authors. Licensee MDPI, Basel, Switzerland. This article is an open access article distributed under the terms and conditions of the Creative Commons Attribution (CC BY) license (<https://creativecommons.org/licenses/by/4.0/>).

## 1. Introduction

Triassic sandstones form important hydrocarbon reservoirs in the central North Sea, with production having taken place over several decades [1,2]. Hydrocarbon exploration and production of this play continues to the present day, despite the North Sea Basin now having reached a super-mature phase. The fundamental controls on Triassic reservoir distribution are extensional tectonics, halokinesis, climate, depositional facies and diagenesis, all of which have been extensively studied [2–9]. In contrast, studies of sediment sourcing for the central North Sea Triassic succession have been comparatively scarce, despite provenance playing a fundamental role in controlling the distribution and quality of reservoir sandstones [10]. As a consequence, there are continued uncertainties over the palaeogeographic framework, in particular regarding the respective roles of the most likely source regions, Scotland to the west and Scandinavia to the east (Figure 1), and whether sediment supply was axial, lateral, or a combination of the two [9,11–13].

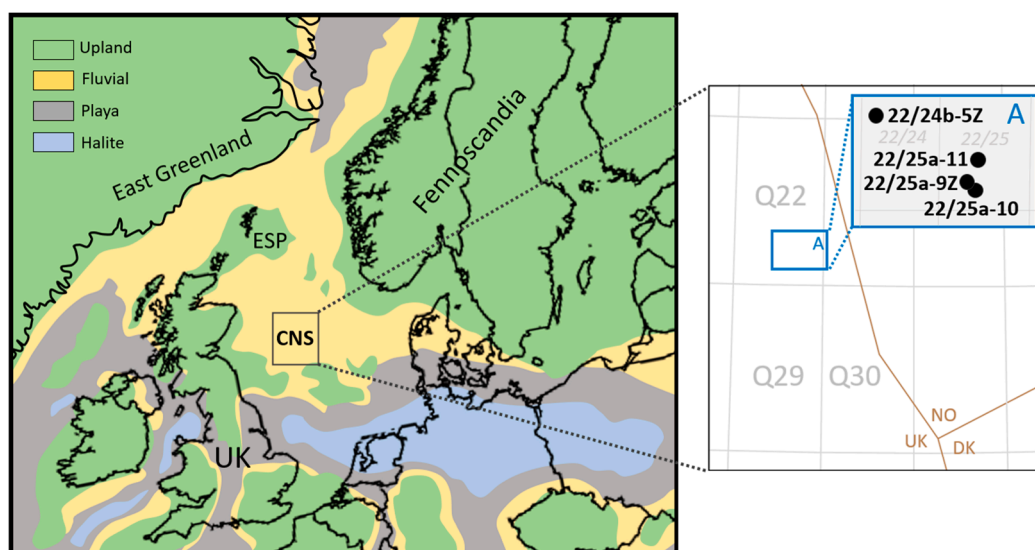


**Figure 1.** Middle Triassic (Judy Sandstone Member) palaeogeographic reconstruction of NW Europe showing location of the study area and wells discussed in this paper, modified from McKie [5].

Establishing provenance of central North Sea Triassic sandstones is especially challenging owing to the extensive diagenetic modification of mineralogy as a result of deep burial. To date, there have been only three published heavy mineral studies of the central North Sea Triassic [14–16]. These were undertaken primarily for correlation purposes since the central North Sea Triassic is characterised by poor palynological recovery and has thus proven difficult to correlate on conventional biostratigraphic grounds except in relatively small areas [17,18]. Heavy mineral suites are extremely restricted in diversity, with only four minerals (apatite, rutile, tourmaline and zircon) being present in significant amounts [14–16]. Reconstructing provenance on the basis of such limited information requires detailed mineral-chemical investigations of the stable components [19]. In this paper, we present isotopic and trace element data from zircon and apatite, in order to place constraints on the location and nature of source regions and the relative importance of first-cycle and recycled detritus for the central North Sea Triassic.

## 2. Geological Background

### 2.1. Structure

During the Triassic, the central North Sea region was located within the Pangean supercontinent, a considerable distance from the Boreal and Tethyan seas (Figure 1), at a latitude of  $\sim 20^\circ$  N [20,21]. The Triassic depocentre of the Central North Sea is superimposed over the site of the Northern Permian Basin [22], where evaporites of the Late Permian Zechstein Group were deposited. In the Triassic, continental clastic sedimentation led to the deposition of red-bed mudstones, siltstones and sandstones above the Zechstein evaporites, which consequently were subject to syn- and post-depositional halokinetic mobilisation. The effects of halokinesis on Triassic sediment thickness and facies distribution have been the subject of considerable debate [3,4,11,23–25]. To generalise, sedimentation models can be grouped into two categories: (a) initially unconfined sands that are now only preserved within salt synclines, and (b) confined sediment pathways that were limited to salt-withdrawal pod synforms that resulted from vertical and/or lateral diapirism. Variations in salt thickness, reflecting the burial of remnant topography during the Permian [26], resulted in localised instances of grounding of mini-basins onto the sub-salt substrate at points of complete salt withdrawal, typically upon horsts comprising Early Permian sandstones of the Rotliegend Group [5]. Such grounding led to spatial differences in accommodation space and the generation of localised intra-Triassic unconformities [27]. Resultant halokinetic modification of the intra-basinal topography potentially influenced sediment

distribution patterns, and resultant highs separating mini-basins may have exposed older Triassic sequences susceptible to sedimentary reworking. Whilst extensional faulting affected the Central Graben during the Early Triassic [28], rifting was focused primarily on the Norwegian-Danish Basin and Viking Graben areas [29,30], with the present-day configuration of the Central Graben largely reflecting post-Triassic westwards-directed rift migration [31]. Relatively complete (Early Triassic to Rhaetian) sections are found only in these graben areas, with the Triassic being truncated over most of the central North Sea by post-Triassic unconformities.

### 2.2. Stratigraphy

The Triassic succession in the central North Sea is assigned to the Heron Group (Figure 2). Early Triassic strata comprise mudstones and siltstones of the Smith Bank Formation, overlain by the Bunter Sandstone Member [32,33]. Middle-Late Triassic sediments belong to the Skagerrak Formation [34], which Goldsmith et al. [17] further subdivided into mudstone-dominated (Julius, Jonathan and Joshua mudstones) and intervening sandstone-dominated members (Judy, Joanne and Josephine sandstones) in the Q30 area. In parts of the central North Sea, the Bunter Sandstone is separated from the Judy Sandstone Member by the ‘Marnock Shale’ [11], which Archer et al. [35] assigned member status as part of the Smith Bank Formation. Mouritzen et al. [16] showed that the J-nomenclature can be extended into the Culzean and Marnock Field areas in Q22 using a combination of palynological and heavy mineral analysis. Burgess et al. [18] used new processing techniques to enhance palynological recovery, enabling correlation over a wider area and clarifying the ages of the mudstone members in the Skagerrak Formation.

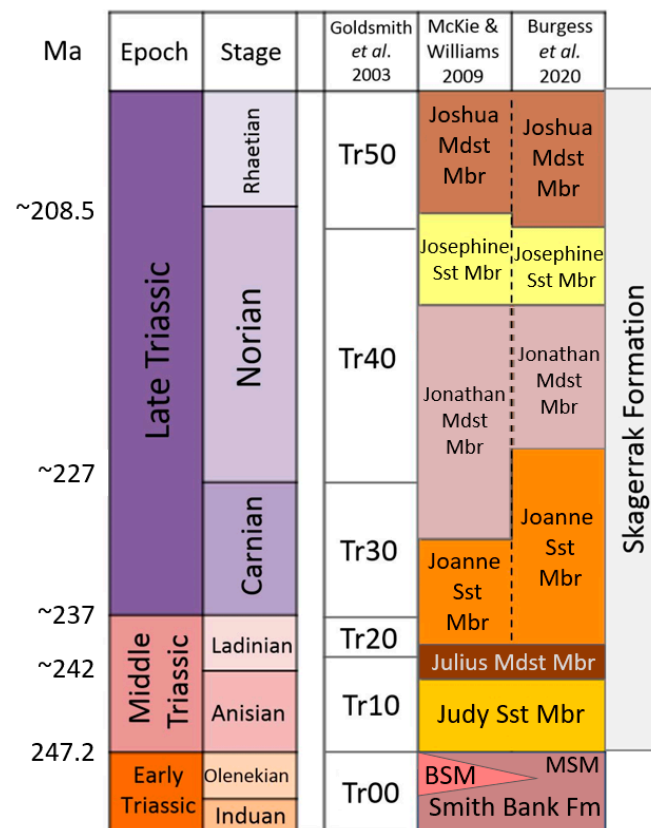


Figure 2. Central North Sea Triassic stratigraphic framework based on Cameron [34], Goldsmith et al. [33], McKie & Williams [21] and Burgess et al. [18]. BSM = Bunter Sandstone Member, MSM = Marnock Shale Member. Timescale from Cohen et al. [36].

### 2.3. Depositional Setting

Whilst Early Triassic deposits were deposited under relatively arid conditions across NW Europe, amelioration of the climate due to the northward drift of Pangaea resulted in the deposition of the Skagerrak Formation under mostly semi-arid conditions during the Middle-Late Triassic [12,35]. However, climatic reconstructions for the Late Triassic suggest that the region occasionally experienced subtropical arid to tropical summers [37], particularly during the Carnian [5,38].

Channelised, sheet-flood and splay sandstones of the Heron Group were deposited by distributive fluvial or terminal fluvial dryland systems [5,9,11], whilst argillaceous intervals of the Skagerrak Formation were largely deposited under floodplain, playa or marshy palustrine conditions [18,35,39,40]. Goldsmith et al. [33], Archer et al. [2] and McKie [5] attributed the cyclical nature of the Skagerrak Formation, represented by the alternation of sandstone- and mudstone-dominated intervals, to climatic changes. However, there are contrasting opinions on the nature of the climatic forcing: Goldsmith et al. [33] suggested that the mudstones were deposited in humid lacustrine or swamp conditions and that the sandstone members represent more arid conditions, whereas Archer et al. [2] and McKie [5] proposed that the sandstone members were deposited during wetter climate phases during basinward expansion of the fluvial systems, with the mudstone members being deposited during more arid conditions when the fluvial systems contracted. However, the detailed palaeoenvironmental study carried out by Burgess et al. [40] showed that there is no simple relationship between climate change and sandstone or mudstone development in the basin centre, and that hydrological conditions varied between different mudstone members.

### 2.4. Hinterland Uplift

Recent tectonothermal studies [41–44] have provided constraints on Triassic uplift events in Scotland and Scandinavia. In northern Scotland, progressive exhumation occurred throughout the Mesozoic with the uplift of the western Highlands occurring at 245–225 Ma (earliest Anisian to early Norian) [42,45]. In southern Fennoscandia, cooling associated with rift-flank uplift was initiated during Induan to the earliest Anisian times [46], in conjunction with Late Triassic faulting along major lineaments [43,44]. In Norway, exhumation is estimated to have removed ~1.5–3 km of overburden in the form of Caledonian nappes and possibly late Palaeozoic to Early Triassic sediments [46]. This exhumation exposed metamorphic basement during the Late Triassic across parts of SW Norway and the Utsira High [47]. On the basis of this evidence, therefore, sediment could have been supplied to the central North Sea region from both east and west.

## 3. Previous Provenance Studies

Petrographic studies indicate that the Skagerrak sandstones of UK Quadrant 30 are typically subarkosic–arkosic and contain lithic fragments indicating low- to high-grade metamorphic input [8]. Triassic sandstones of UK Quadrant 22 have similar compositions [48], except that lithic fragments are dominantly of sedimentary origin, with igneous and metamorphic lithologies being subordinate [49]. Feldspar contents have been variably reduced during burial diagenesis [8].

Jeans et al. [14] determined the proportions of detrital minerals within heavy mineral assemblages from twenty-one central North Sea wells, and observed fluctuations in apatite and zircon abundances that they attributed to changes in provenance. However, apatite and zircon have contrasting hydrodynamic behaviour owing to their different densities, and it is therefore likely that at least some of the observed variations resulted from differing hydraulic conditions at the time of deposition [50–52].

In order to obviate hydrodynamic and diagenetic controls in heavy mineral assemblage compositions, Mange-Rajetzky [15] focused on varietal studies, whereby variations shown by individual mineral components are quantified. On the basis of grain morphologies, an intra-Skagerrak Formation marker horizon was recognised, separating polycyclic, well-rounded detritus in the earlier part of the succession from less-rounded, apparently

first-cycle material in the later Triassic. Mange-Rajetzky [15] considered this change to reflect a change from reworking of Permian aeolianites to the influx of Fennoscandian-sourced material introduced by fluvial systems. However, it is possible that the observed morphological changes reflect a transition from aeolian-dominated to fluvially dominated transport processes, rather than to provenance.

The existence of systematic variations in heavy mineral grain morphology identified by Mange-Rajetzky [15] was verified by Mouritzen et al. [16] in their stratigraphic study on Triassic sandstones in the Culzean Field and adjacent areas. They observed that the influx of apparently first-cycle detritus with very low apatite roundness coincided with the consistent presence of trace amounts of the ultramafic/mafic indicator mineral chrome spinel. This relationship confirms that the change in mineral morphology was at least in part related to a change in provenance, attributed to a switch in supply from the Scottish margin to Fennoscandia [15,16]. This inference was based on the distribution of ophiolites in Scandinavia and Scotland, which are widely distributed in southwestern Norway [53] but less common and unfavourably situated in the Scottish Caledonides (Highland Border Complex of the Midland Valley of Scotland, plus Unst in Shetland; Bluck [54]; Crowley and Strachan [55]). On the basis of biostratigraphic correlation between Culzean and Q30, Mouritzen et al. [16] showed that the sandstones with high apatite roundness and scarce chrome spinel represent the Judy Sandstone Member (and the underlying Bunter Sandstone Member), whereas the sandstones with low apatite roundness and common chrome spinel belong to the Joanne Sandstone Member. The intervening Julius Mudstone Member, which is relatively sand-rich in the Culzean area, has a similar character to the Judy Sandstone Member although has some intermediate features, such as gradually reducing apatite roundness [16].

A major problem in linking central North Sea Triassic heavy mineral assemblages to provenance is that dissolution of unstable and metastable minerals during burial diagenesis has led to impoverished assemblages and a consequent loss of provenance information. In this paper, we augment existing heavy mineral assemblage and textural data with U-Pb geochronological data from two of the stable detrital components, zircon and apatite, plus trace element mineral chemical data from apatite, in order to provide more definitive constraints on provenance. Although detrital zircon geochronology is now commonplace in sediment provenance studies worldwide, for example in Indonesia [56], Australia [57], the Middle East [58], east Greenland [59] and North America [60], applications have been comparatively scarce in a central North Sea context, having been restricted to just two studies on Devonian and Carboniferous sandstones in the UK and Norwegian sectors [61,62]. U-Pb studies of detrital apatite are, by contrast, in their infancy, and this study is to our knowledge the first time the method has been used in the North Sea. The use of apatite as a provenance tracer differs from zircon in three important respects: (i) apatite is strongly susceptible to dissolution during surficial weathering, and therefore is significantly less readily recycled; (ii) it occurs in a wider range of source lithologies than zircon, and therefore provides more comprehensive information on provenance, and (iii) it has a lower crystallisation temperature [63]. The temperature sensitivity of the U-Pb system is governed by the diffusion of Pb, with the partial retention zone for Pb having been experimentally determined as ~ 350–475 °C [64]. Furthermore, since apatite is prone to dissolution-reprecipitation during metamorphism [65], U-Pb ages of apatite in metamorphic rocks may reflect the most recent reordering of the crystal lattice [63]. Integrating provenance information from zircon and apatite, therefore, offers the opportunity to evaluate the relative importance of first-cycle and recycled detritus as well as enabling the identification of a wider range of source lithologies than zircon alone.

In order to achieve this purpose, zircon and apatite U-Pb age data have been acquired from two wells (22/25a-9Z and 22/25a-10) in the Culzean Field, and from Marnock Field well 22/24b-5Z. These wells were all included in the heavy mineral correlation study by Mouritzen et al. [16], and 22/24b-5Z was also a key well in the study by Mange-Rajetzky [15]. Five samples, three from 22/24b-5Z, one from 22/25a-9Z and one

from 22/25a-10, were selected for geochronological analysis in order to cover the observed changes in heavy mineral characteristics between the Bunter Sandstone Member, the Judy Sandstone Member, and the Joanne Sandstone Member. The positions of the five analysed samples are shown on heavy mineral stratigraphic profiles in Figure 3. Apatite trace element data were acquired from the same sample set in order to establish source lithologies as well as ages.

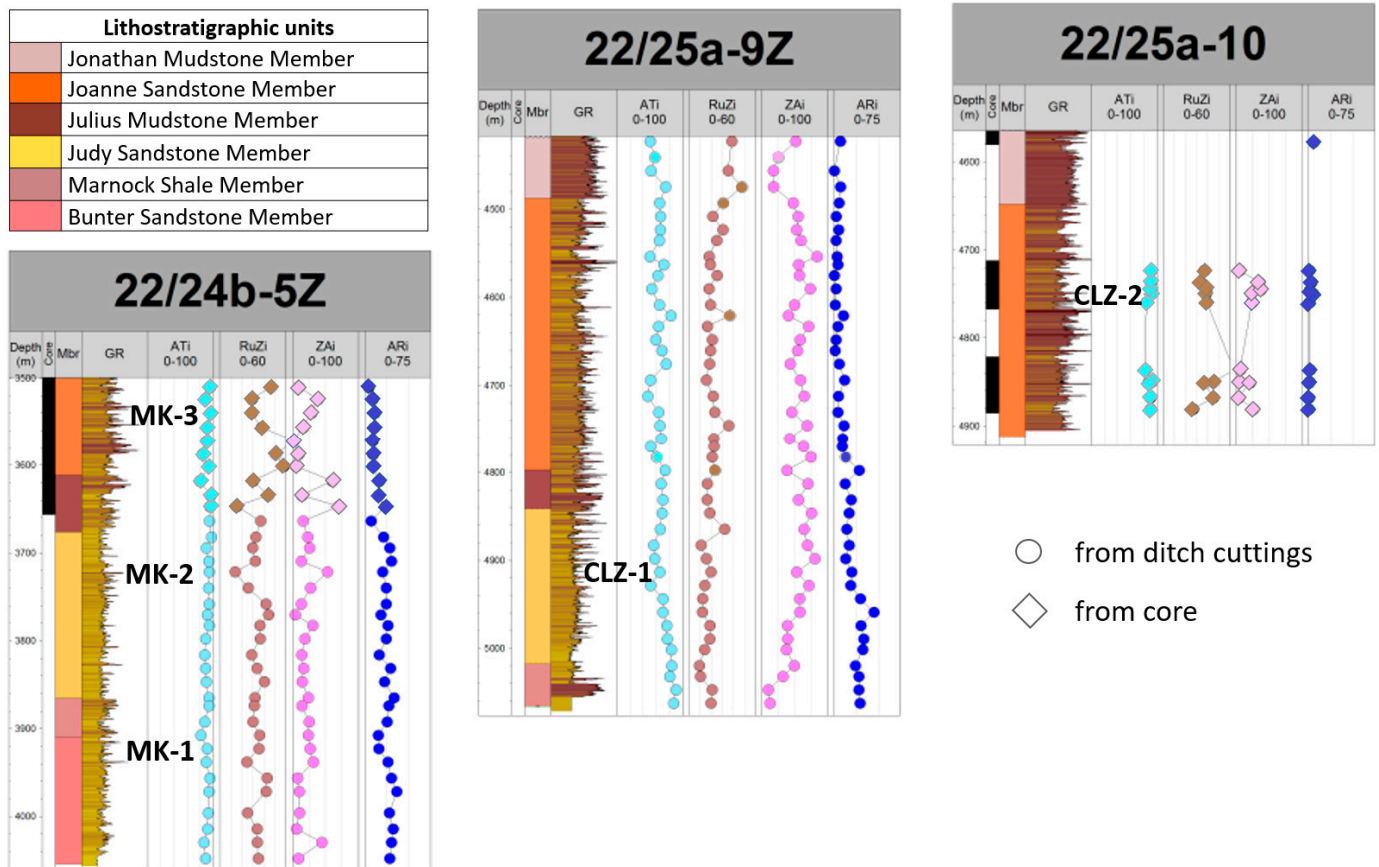


**Figure 3.** Stratigraphic variations in key heavy mineral parameters for the Triassic in the three wells discussed in this paper, showing locations of samples with zircon and apatite isotopic and trace element data. Profiles are based on data from Greig [66], consistent with previous results of Mouritzen et al. [16]. ATi = apatite:tourmaline index, RuZi = rutile:zircon index, ZAi = zircon:apatite index, ARi = apatite roundness index; see Morton and Hallsworth [67], Morton et al. [68] and Mouritzen et al. [16] for definitions. MK-1, MK-2, MK-3, CLZ-1 and CLZ-2: see Supplementary Materials.

#### 4. Analytical Methods

Zircon U-Pb age data were obtained at the Central Analytical Facility (CAF), Stellenbosch University, by laser ablation—single collector—magnetic sectorfield—inductively coupled plasma—mass spectrometry (LA-SF-ICP-MS) employing a Thermo Finnigan Element2 mass spectrometer coupled to a NewWave UP213 laser ablation system. All age data presented here were obtained by single spot analyses with a spot diameter of 30  $\mu\text{m}$  and a crater depth of approximately 15–20  $\mu\text{m}$ , corresponding to an ablated zircon mass of approximately 150–200 ng. The methods employed for analysis and data processing are described in detail by Gerdes and Zeh [69] and Frei and Gerdes [70]. For quality control, the Plešovice [71] and M127 [72,73] zircon reference materials were analysed, and the results were consistently in excellent agreement with the published ID-TIMS ages. Full analytical details and the results for all quality control materials analysed are reported in Table 1. Plotting of Concordia diagrams was performed using Isoplot/Ex 3.0 [74] and probability-density plots (Figure 4) were generated using AgeDisplay [75].

**Table 1.** LA-SF-ICP-MS U-Th-Pb dating methodology for zircons discussed in this paper.

<b>Laboratory &amp; Sample Preparation</b>	
Laboratory name	Central Analytical Facility, Stellenbosch University
Sample type/mineral	Detrital zircons
Sample preparation	Conventional mineral separation, 1 inch resin mount, 1 µm polish to finish
Imaging	CL, Zeiss Merlin, 10 nA, 15 mm working distance
<b>Laser ablation system</b>	
Make, Model & type	Resonetics Resolution S155, ArF Excimer
Ablation cell & volume	Laurin Technology S155 double Helix large volume cell
Laser wavelength	193 nm
Pulse width	20 ns
Fluence	Approx. 2 J/cm <sup>-2</sup>
Repetition rate	5.5 Hz
Spot size	30 µm
Sampling mode/pattern	30 µm single spot analyses
Carrier gas	100% He, Ar make-up gas combined using a T-connector close to double Helix sampling funnel
Pre-ablation laser warm-up (background collection)	3 cleaning shots followed by 20 s background collection
Ablation duration	15 s
Wash-out delay	15 s
Cell carrier gas flow	300 mL/min He & 0.06 mL/min N <sub>2</sub>
<b>ICP-MS Instrument</b>	
Make, Model & type	Thermo Finnigan Element2 single collector HR-SF-ICP-MS
Sample introduction	Via conventional tubing
RF power	1350 W
Make-up gas flow	1.0 L/min Ar
Detection system	Single collector secondary electron multiplier
Masses measured	202, 204, 206, 207, 208, 232, 233, 235, 238
Integration time per peak	4 ms
Total integration time per reading	1 sec (represents the time resolution of the data)
Sensitivity	30,000 cps/ppm Pb
Dead time	6 ns
<b>Data Processing</b>	
Gas blank	20 s on-peak
Calibration strategy	GJ-1 used as primary reference material, M127 & 91500 used as secondary reference material (Quality Control)

Table 1. Cont.

<b>Laboratory &amp; Sample Preparation</b>	
Reference Material info	M127 (Nasdala et al. [72]; Mattinson [73]), 91500 (Wiedenbeck et al. [76]), GJ-1 (Jackson et al. [77])
Data processing package used/Correction for LIEF	In-house spreadsheet data processing using intercept method for LIEF correction
Mass discrimination	Standard-sample bracketing with $^{207}\text{Pb}/^{206}\text{Pb}$ and $^{206}\text{Pb}/^{238}\text{U}$ normalized to reference material GJ-1
Common-Pb correction, composition and uncertainty	204-method, Stacey & Kramers [78] composition at the projected age of the mineral, 5% uncertainty assigned
Uncertainty level & propagation	Ages are quoted at $2\sigma$ absolute, propagation is by quadratic addition. Reproducibility and age uncertainty of reference material and common-Pb composition uncertainty are propagated.
Quality control/Validation	91500: Concordia age = $1072.9 \pm 6.2$ ( $2\sigma$ , $n = 10$ , MSWD = 0.28) M127: Wtd Concordia age = $528.8 \pm 2.1$ ( $2\sigma$ , $n = 15$ , MSWD = 0.32)
<b>Other information</b>	For detailed method description see Frei & Gerdes [70]

Apatite U–Pb age data were also obtained at CAF, using the same equipment as in the zircon U–Pb analysis. The age data were obtained by single spot analyses with a spot diameter of 43  $\mu\text{m}$  and a crater depth of approximately 15–20  $\mu\text{m}$ . The methods employed for analysis and data processing are similar to those described in detail by Gerdes and Zeh [69] and Frei and Gerdes [70]. The Madagascar apatite [79,80] was used as primary calibration material. For quality control, the Durango apatite [81] was analysed, and the results were consistently in good agreement with the published ages. Common Pb correction for apatite analyses followed the  $^{207}\text{Pb}$  method outlined by Chew et al. [81], using iterative age estimates and the Stacey and Kramers [78] model. Full analytical details and the results for all quality control materials analysed are reported in Table 2. Probability-density plots (Figure 4) were generated using AgeDisplay [75].

Trace element contents of apatite crystals in polished mounts were determined by laser ablation—inductively coupled plasma—mass spectrometry (LA-ICP-MS) at CAF. The LA-ICP-MS system consists of an excimer laser ablation system (ASI Resolution SE-S155 utilising a ATL Atlex laser source emitting at 193 nm) coupled to a Agilent 7700ce quadrupole ICP-MS. All trace element data were obtained by single spot analysis using 40  $\mu\text{m}$  beam diameters and a laser repetition rate of 8 Hz. A laser energy of 2.5 mJ at 25% attenuation was employed, resulting in a fluence of 2 J/cm<sup>2</sup>, as determined directly above the ablation cup with a hand-held external energy meter. Ablation was performed using a S155 dual-volume ablation cell (Laurin Technic, Canberra, Australia) in He that was mixed in a conical ablation cup into the argon sample gas of the mass spectrometer and N<sub>2</sub> as make-up gas. Gas flows for He, Ar and N<sub>2</sub> were 330 mL/min, 940 mL/min and 5 mL/min, respectively. The isotope used for internal standardization was  $^{43}\text{Ca}$  (with stoichiometric concentrations used for apatite) and the NIST610 standard reference glass (values from Jochum and Nehring [82]) was used as primary calibration standard. In a typical analytical sequence, one primary calibration standard was analysed, followed by 10 to 15 unknowns, secondary standards for quality control purposes, then one primary calibration standard, and so on. Prior to each analysis the sample surface was cleaned from contamination with 3 laser pulses, followed by 15 s wash-out time. Each subsequent



analysis commenced with 15 s measurement of the gas blank prior to ablation, followed by 15 s of ablation and 40 s wash-out time. Data acquisition was performed in time-resolved mode by peak hopping measuring 1 sample per peak. Twenty five isotopes ( $^{24}\text{Mg}$ ,  $^{43}\text{Ca}$ ,  $^{51}\text{V}$ ,  $^{55}\text{Mn}$ ,  $^{56}\text{Fe}$ ,  $^{88}\text{Sr}$ ,  $^{89}\text{Y}$ ,  $^{137}\text{Ba}$ ,  $^{139}\text{La}$ ,  $^{140}\text{Ce}$ ,  $^{141}\text{Pr}$ ,  $^{146}\text{Nd}$ ,  $^{147}\text{Sm}$ ,  $^{151}\text{Eu}$ ,  $^{157}\text{Gd}$ ,  $^{159}\text{Tb}$ ,  $^{163}\text{Dy}$ ,  $^{165}\text{Ho}$ ,  $^{166}\text{Er}$ ,  $^{169}\text{Tm}$ ,  $^{174}\text{Yb}$ ,  $^{175}\text{Lu}$ ,  $^{208}\text{Pb}$ ,  $^{232}\text{Th}$ ,  $^{238}\text{U}$ ) were analysed. Reduction in the time-resolved data and concentration calculations were subsequently performed off-line using the GLITTER software package ([www.glitter-gemoc.com](http://www.glitter-gemoc.com)). Time-resolved analytical signals for each analysis were meticulously checked and acquisitions were discarded when sudden signal changes indicated concomitant analysis of matrix minerals or the laser beam had drilled in a different phase. One analysis of the NIST612, BHVO and the BCR reference glasses were performed with every 10 to 15 unknowns for quality control (QC) and the results are consistently within  $2\sigma$  of the average concentrations reported by Jochum and Nehring [83,84]. The detection limit for most of the elements is in the lower ppb to mid-ppt range.

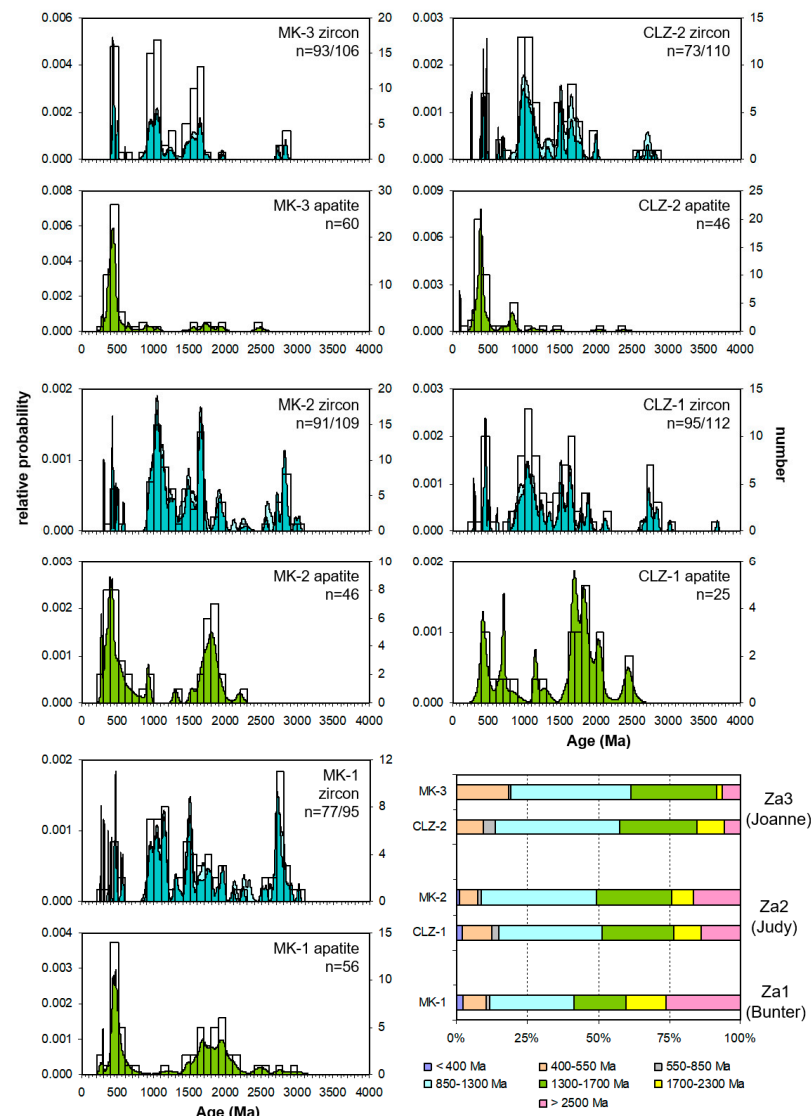


**Figure 4.** Probability-density plots of zircon and apatite U-Pb ages. For zircon, ‘n’ = number of zircons with <10% discordance in the total zircon population (for example, n = 93/106 indicates 93 concordant ages from a total of 106 analyses). For apatite, ‘n’ = number of analyses. Bar chart in bottom right shows the relative abundance of the main components of the zircon age spectra. See Figure 3 for location of samples MK-1, MK-2, MK-3, CLZ-1 and CLZ-2.

**Table 2.** LA-SF-ICP-MS U-Pb dating methodology for apatites discussed in this paper.

<b>Laboratory &amp; Sample Preparation</b>	
Laboratory name	Central Analytical Facility, Stellenbosch University
Sample type/mineral	Detrital apatites
Sample preparation	Conventional mineral separation, 1 inch resin mount, 1 $\mu\text{m}$ polish to finish
Imaging	CL, LEO 1430 VP, 10 nA, 15 mm working distance
<b>Laser ablation system</b>	
Make, Model & type	ASI Resolution S155, ArF Excimer Coherent CompexPro 110
Ablation cell & volume	Laurin Technology S155 double helix large volume cell
Laser wavelength	193 nm
Pulse width	20 ns
Fluence	2.8 J/cm <sup>-2</sup> (measured with external energy meter above sample funnel)
Repetition rate	5.5 Hz
Spot size	43 $\mu\text{m}$
Sampling mode/pattern	20 $\mu\text{m}$ single spot analyses
Cell carrier gas	100% He, Ar and N <sub>2</sub> make-up gases combined using injectors into double Helix sampling funnel
Pre-ablation laser warm-up (background collection)	3 cleaning shots followed by 20 s background collection
Ablation duration	20 s
Wash-out delay	15 s
Cell carrier gas flows	290 mL/min He
<b>ICP-MS Instrument</b>	
Make, Model & type	Thermo Finnigan Element2 single collector HR-SF-ICP-MS
Sample introduction	Via Nylon 10 tubing
RF power	1350 W
Make-up gas flow	910 mL/min Ar & 2 mL/min N <sub>2</sub>
Detection system	Single collector secondary electron multiplier
Masses measured	202, 204, 206, 207, 208, 232, 233, 235, 238
Integration time per peak	4 ms
Total integration time per reading	1 s ( <i>represents the time resolution of the data</i> )
Sensitivity	30,000 cps/ppm Pb
Dead time	6 ns
<b>Data Processing</b>	
Gas blank	20 s on-peak
Calibration strategy	Madagascar apatite used as primary reference material, Durango apatite used as secondary reference material (Quality Control)

Table 2. Cont.

<b>Laboratory &amp; Sample Preparation</b>	
Reference Material info	Madagascar apatite (Thomson et al. [79], Cochrane et al. [80]), R10 (Chew et al. [81])
Data processing package used/Correction for LIEF	In-house spreadsheet data processing using intercept method for LIEF correction
Mass discrimination	Standard-sample bracketing with $^{207}\text{Pb}/^{206}\text{Pb}$ and $^{206}\text{Pb}/^{238}\text{U}$ normalized to reference material SRQ36
Common-Pb correction, composition and uncertainty	Iterative $^{207}\text{Pb}$ correction method of Chew et al. [81]. Data are filtered to exclude imprecise analyses (>20% age uncertainty, $2\sigma$ ) and analyses with very high levels of non-radiogenic lead (>80% $f_{206}$ , which is the fraction of $^{206}\text{Pb}$ that is non-radiogenic).
Uncertainty level & propagation	Ages are quoted at $2\sigma$ absolute, propagation is by quadratic addition. Reproducibility and age uncertainty of reference material and common-Pb composition uncertainty are propagated.
Quality control/Validation	Durango apatite: Wt mean $^{206}\text{Pb}/^{238}\text{U}$ age = $31.9 \pm 2.8$ Ma ( $2\sigma$ MSWD = 0.89)
<b>Other information</b>	For detailed method description see Frei & Gerdes [70]

Apatite compositions, and especially their rare-earth element (REE) contents, are known to be sensitive to the nature of the host rock in which they formed (see summary by O'Sullivan et al. [63]), and a variety of plots have been proposed as diagnostic indicators of their origin. These include La/Nd versus (La + Ce + Pr)/ $\Sigma$ REE [85,86], Sr versus Y [87], and  $\Sigma$ REE versus Ce/Yb [87]. These plots are all potentially useful in linking detrital apatites to their igneous source lithologies. However, they fail in one important respect, since apatite can also form in metamorphic environments. This omission has been addressed by O'Sullivan et al. [63], who showed that comparisons of Sr/Y and total LREE (light rare earth elements) enable discrimination of metamorphic apatites from igneous apatites while retaining the ability to type igneous apatites to their original sources. Consequently, the data acquired during this study have been plotted on Sr/Y versus total LREE diagrams (Figure 5) to identify the main apatite sources.

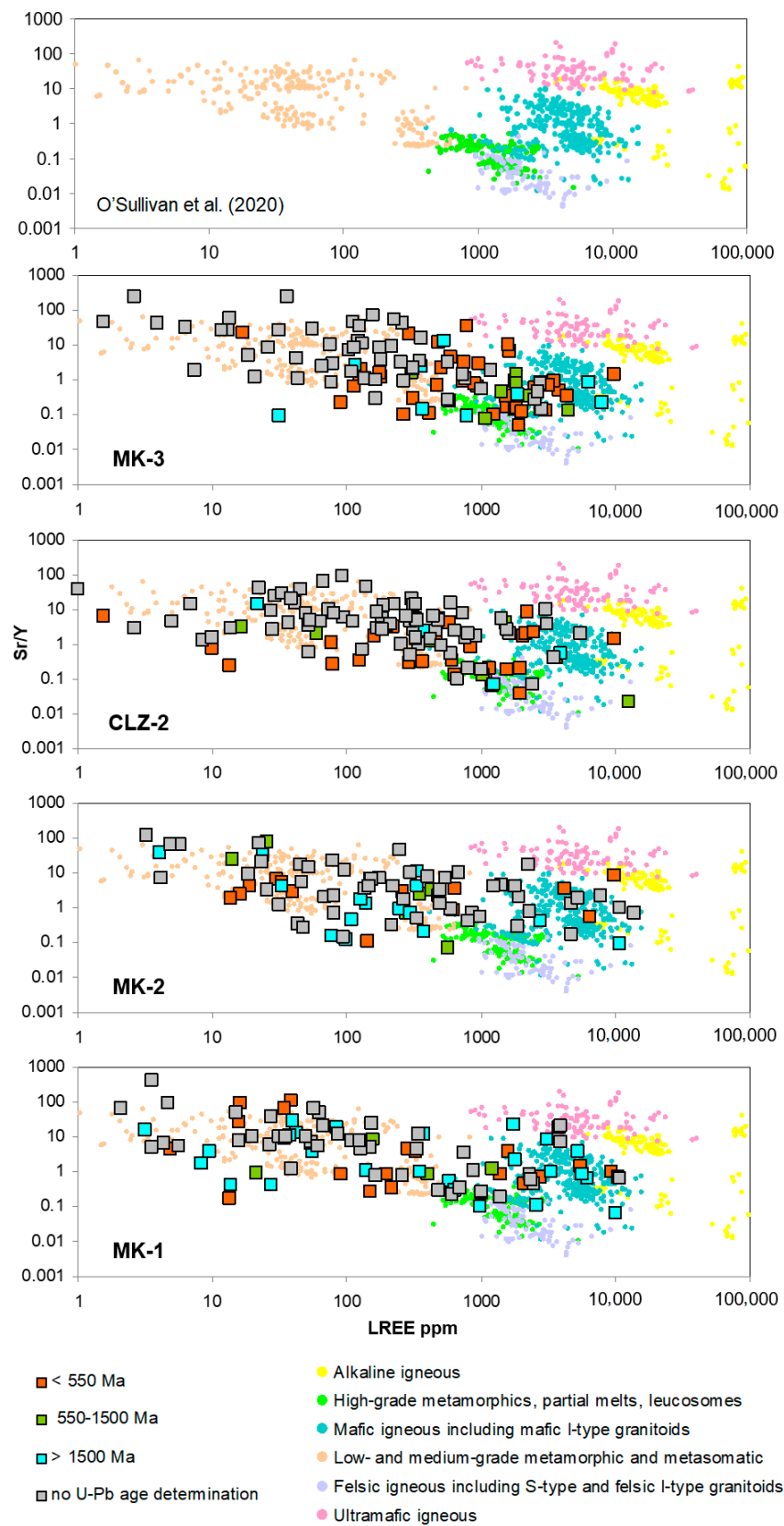


**Figure 5.** Apatite trace element data from samples MK-1, MK-2, MK-3 and CLZ-2 shown on Sr/Y—light rare earth element (LREE; La + Ce + Pr + Nd) diagrams. Data are coded to show the main age groups and which did not yield useful age data. Detrital compositions are compared with those from apatite parent rocks as compiled by O’Sullivan et al. [63].

## 5. Results

### 5.1. Zircon Geochronology

Three zircon associations have been recognized. Zircon association 1 (Za1) characterises sample MK-1 from the Bunter Sandstone Member in well 22/24b-5Z. Zircon association 2 (Za2) is identified in samples MK-2 and CLZ-1 from the Judy Sandstone Member of wells 22/24b-5Z and 22/25a-9Z. Zircon association 3 (Za3) is found in samples MK-3 and CLZ-2 from the Joanne Sandstone Member of wells 22/24b-5Z and 22/25a-10, respectively (Figure 4).

The primary defining feature of Za1 is the large Archaean component, which forms 26% of the near-concordant population. This group displays a dominant peak at ca. 2700 Ma and ranges from  $2501 \pm 19$  to  $3012 \pm 18$  Ma. A prominent cluster also occurs at 900–1150 Ma, contributing 25% of the total population and displaying peaks at ca. 1060 and 1150 Ma. In addition, there is a distinct peak at ca. 1500 Ma, together with a small number of Palaeozoic grains (<9%). The Palaeozoic component is wide-ranging, mostly of Ordovician age (453–488 Ma), but two zircons with younger ages (Late Carboniferous,  $308 \pm 4$  Ma, and Permian,  $266 \pm 3$  Ma) were also detected. There is also a minor Ediacaran component ( $543 \pm 6$  and  $568 \pm 6$  Ma).

Association Za2 is dominated by Proterozoic zircons (74–77%), the strongest groupings being ca. 900–1300 Ma (main peak at ca. 1050) and 1350–1700 Ma (main peak at ca. 1650 Ma). There is also an important but subsidiary Archaean component, mostly within the 2700–2880 Ma interval but extending back to  $3683 \pm 16$  Ma, which forms 14–16% of the overall concordant population. Palaeozoic zircons, mostly between 424–492 Ma, form 7–14% of the concordant population. The youngest zircon is dated at  $286 \pm 3$  Ma (Permian), and there are two Carboniferous zircons ( $307 \pm 4$  Ma and  $309 \pm 4$  Ma), similar in age to the  $308 \pm 4$  Ma grain in sample MK-1.

Association Za3 is distinguished from Za1 and Za2 by the lower proportion of zircons with ages > 1860 Ma (Palaeoproterozoic-Archaean), which form only 7–9% of the populations. The largest group has ages between 900–1150 Ma, peaking at ca. 1050 Ma, which forms 39–40% of the concordant populations. There are also notable Proterozoic peaks at ca. 1500 Ma and 1650 Ma. The samples display a subordinate Palaeozoic component (10–14% of the concordant population), which is largely Silurian in age but extends back to the late Cambrian (421–502 Ma).

### 5.2. Apatite Geochronology

U-Pb apatite age data for the Bunter, Judy and Joanne sandstone units all display a strong Caledonian cluster between ca. 400–500 Ma (Figure 4). However, the proportion of Palaeozoic ages is considerably larger in samples MK-3 and CLZ-2 (Joanne Sandstone Member), which have essentially unimodal apatite populations. In contrast, Palaeozoic varieties only form 16–44% and 36% of the population in samples MK-1, MK-2 and CLZ-1 (Bunter Sandstone Member and Judy Sandstone Member). These samples have bimodal apatite age patterns, the Palaeozoic group being subordinate to Proterozoic apatites in the 1500–2000 Ma age range.

### 5.3. Apatite Trace Elements

Trace element data for four of the five samples are shown using Sr/Y-LREE plots in Figure 5, coded with their U-Pb dates to determine if there are systematic differences in compositions depending on age. The results from one sample (CLZ-1) are not shown since trace element analysis was unsuccessful. Four apatite groups are plotted per sample, apatites with ages < 550 Ma (broadly corresponding to the Caledonian orogenic cycle), those with ages > 1500 Ma, the small number with intervening ages, and those that did not yield useful U-Pb isotopic data.

In all samples, many of the apatites with compositions that correspond to those found in low- to medium-grade metamorphic and metasomatic rocks fail to yield useful U-Pb isotopic data. This appears to be a typical feature of low- and medium-grade metamorphic

apatites [63,88], because they tend to be poor in U and rich in Pb<sub>c</sub> (common Pb). None of the samples have apatites with ultramafic or alkaline igneous compositions, and those with felsic igneous compositions are also very scarce.

In the two Joanne Sandstone Member samples (MK-3 and CLZ-2), apatites that fall in the dominant age group (<550 Ma) mostly correspond to mafic igneous lithologies (including mafic I-type granitoids), with a substantial number having low- to medium-grade metamorphic and metasomatic compositions. The relatively small numbers of older apatites do not fall in any particular field.

In the samples with large numbers of Meso- and Palaeoproterozoic apatites (Judy Sandstone Member, MK-2, and Bunter Sandstone Member, MK-1), the young apatite group has compositions that correspond to low- and medium-grade metamorphic rocks as well as mafic igneous lithologies. A large number of the Meso- and Palaeoproterozoic apatites also have low- and medium-grade metamorphic compositions. Mafic igneous Meso- and Palaeoproterozoic apatites are also common in MK-1 but are less apparent in MK-2.

## 6. Interpretation

### 6.1. Zircon

The Archaean component is arguably the most significant part of the detrital zircon population, because Archaean zircon ages are locally abundant within Scotland (e.g., Friend and Kinny [89]; Cawood et al. [90]), but are sparse in southern and mid-Norway [91]. In Scotland, Archaean-aged basement units are primarily represented by the heterogeneous Lewisian Gneiss Complex that is well exposed across low-lying areas of the Hebridean Terrane. This series of accreted crustal blocks predominantly comprises tonalite-trondhjemite-granodiorite gneisses ranging from amphibolite to granulite facies with subordinate lenses and sheets of mafic-ultramafic material [92,93]. The majority of protoliths were emplaced between ca. 3100–2700 Ma [93] and were heavily deformed between ca. 2600 and ca. 2800 Ma. Inliers of ‘Lewisianoid’ orthogneisses tentatively correlated with the Lewisian Gneiss Complex form basement to the Moine succession of the Northern Highland Terrane (e.g., Ramsay [94]; Mendum and Noble [95]), although these outcrops are highly limited in extent. Such inliers are also present across northern areas of the Shetland Islands, as are ca. 2750–2730 Ma granitic gneisses [96] that are the most easterly manifestation of the Archaean Faroe-Shetland terrane that forms the basement to the basins west of Shetland and links with the Rae Craton of central Greenland [97] (terrane locations shown in Figure 6). This Greenland complex consists of amalgamated orthogneiss-dominated terranes derived from protoliths formed during 2950–2630 Ma that are now characterised by granulite and amphibolite facies [98,99]. However, whereas the oldest published protolith ages for the Lewisian Gneiss in Scotland are ca. 3100 Ma [100], the Amîtsoq gneisses of the North Atlantic Craton, West Greenland have yielded considerably older protolith ages of >3700 Ma [101].

Zircons of Archaean age are also locally abundant within Precambrian and Palaeozoic sediments of Scotland, such as the Devonian Old Red Sandstone (ORS) west of Shetland [102,103], Upper ORS deposits of the Inner Moray Firth [103], the Appin, Argyll and Southern Highland groups of the late-Neoproterozoic to Ordovician Dalradian Supergroup and the contiguous Highland Border Complex [90,104,105], and the Precambrian Stoer and Sleat Groups of the Torridonian sandstone in northwest Scotland [106].

Archaean basement complexes in Norway are limited to distal northern regions such as West Troms and Lofoten, where the oldest published U-Pb zircon age is  $2885 \pm 20$  Ma [108]. South of here, the only Archaean records are from zircons in the Caledonian Nappes and supracrustal rocks [91]. Zircons yielding Archaean ages have been reported from peridotites within the Western Gneiss Region [109], early Palaeozoic sediments of SW Norway [110], the Upper Allochthon of Mid-Norway [111], supracrustal sequences of Telemarkia [112], and the Dala Sandstone of SW Sweden [113]. In all cases the numbers of Archaean zircons are very minor, indicating that significant Archaean populations in the central North Sea Triassic are unlikely to have been sourced from Scandinavia. However, minor proportions of Archaean zircon should not be automatically correlated with a westerly Scottish source.

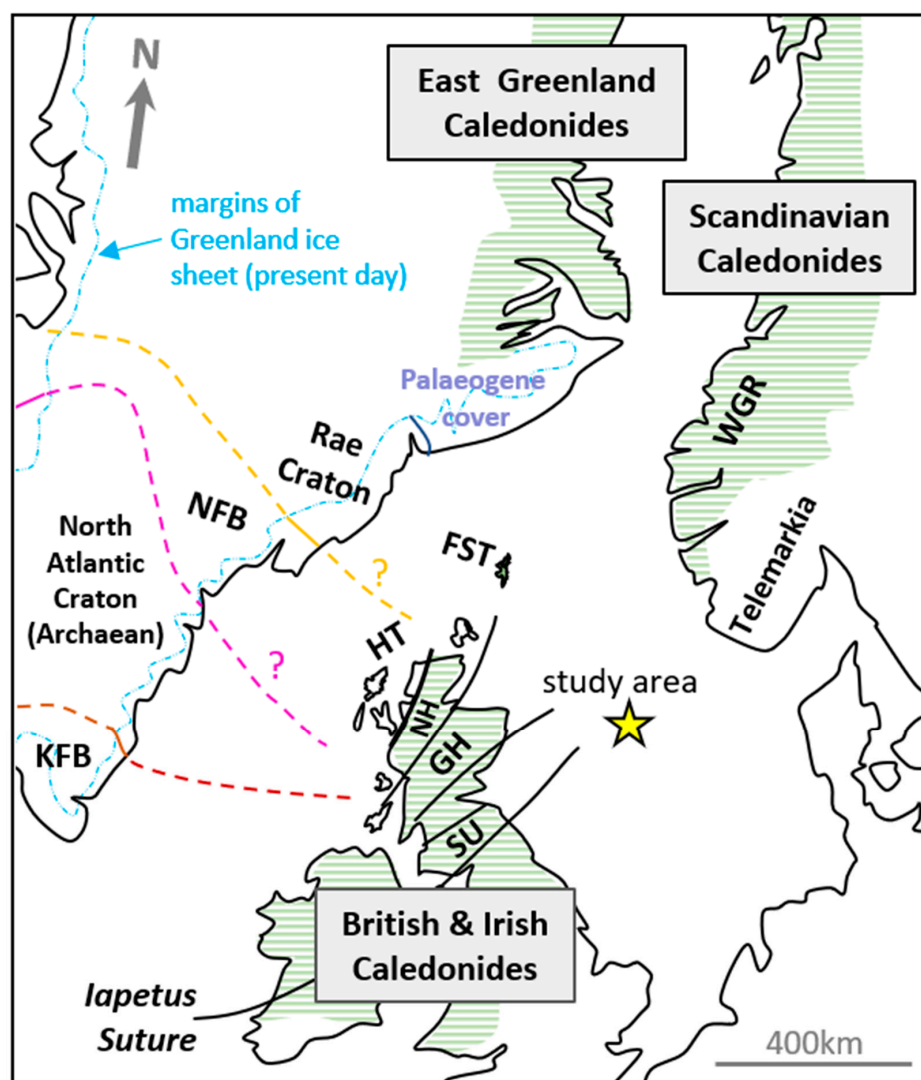


**Figure 6.** Generalised pre-Atlantic drift map reconstruction of the North Atlantic region showing the extent of the Caledonide orogenic belt (dashed green fill), and the location of terranes discussed within the main text. Abbreviations: FST, Faroe-Shetland Terrane; GH, Grampian Highland Terrane; HT, Hebridean Terrane; KFB, Ketilidian Fold Belt; NH, Northern Highland Terrane; NFB, Nagssugtoqidian Fold Belt; SU, Southern Uplands Terrane; WGR, Western Gneiss Region. Based on Dawes [107], Holdsworth et al. [97], and Kinny et al. [96].

The relatively large proportion of Archaean zircons in the Bunter Sandstone Member and Judy Sandstone Member, therefore, indicates ultimate derivation either from Scotland or a more distal source such as Greenland, and the marked decrease in such zircons in the Joanne Sandstone Member is consistent with a switch to sourcing dominantly from Scandinavia, as previously suggested by Gray et al. [9]. The associated mid-Proterozoic zircons are less diagnostic, since they can be found in the basement terranes of Scandinavia, sediments of the overlying Caledonian Nappe Domain, and in the Moine and Dalradian metasediments of Scotland. For example, the 1660 Ma peak, which can be attributed to the Labradorian and contemporaneous Gothian orogenies of NE Canada and Fennoscandia, respectively [114,115], is a common zircon age feature of numerous geological units in Norway, Scotland and East Greenland. In Scandinavia, ca. 1660 Ma ages are common within crystalline basement of the Eastern Segment terrane and the Western Gneiss Region [109,116], and in Proterozoic-aged metasediments within allochthons of the Norwegian Caledonide Belt such as the Kalak Nappe [117]. In Scotland, the 1660 Ma peak is recognised from several stratigraphic units in the Moine Supergroup [118,119]

and the Grampian Group and sub-Grampian basement of the Dalradian sequence [90]. In Greenland, 1660 Ma zircon signatures have been obtained from the Krummedal and Eleonore Bay Supergroup metasediments of the East Greenland Caledonides [120,121].

Likewise, the zircon group at ca. 1500 Ma could be attributed to both Scandinavia and Scotland. In southern Norway, juvenile crust formation took place during the ca. 1520–1480 Ma Telemarkian event [122], and zircons of this age are common in the Telemarkia terrane and in metasediments of the Lower Allochthon [91], particularly from the Suldal region, NE of Stavanger [123]. In Scotland, the 1500 Ma zircon group is present in the Moine Supergroup (Loch Eil Group) of the Northern Highland Terrane [118], although is less common in the Dalradian Supergroup [90,119], apart from the Glen Spean sub-group of the central Highlands [124].

The other major zircon group in the Proterozoic part of the Triassic spectra in this study occurs at ca. 900–1150 Ma, which corresponds to the Grenville Orogeny of Laurentia and the coeval Sveconorwegian Orogeny of Fennoscandia [125]. Grenvillian granites are exceptionally Zr-rich, and therefore show greater zircon fertility than other granites elsewhere within the region [126], possibly explaining why 900–1150 Ma zircons are ubiquitous in the central North Sea Triassic. Zircons corresponding to these orogenic events are also found in Moine and Dalradian metasediments of the Scottish mainland and Shetland Islands [90,118,127], and in the Old Red Sandstone deposits of northern Scotland and Orkney [103]. They appear to be somewhat less common in East Greenland, although there are records of peaks at ca. 1140 Ma [59,120,128], which is coeval with the earliest ‘Arendal phase’ of the Sveconorwegian Orogeny [129].

The majority of the Palaeozoic zircon ages in the Triassic sandstones from the Culzean area undoubtedly relate to the Caledonian orogenic cycle that affected the sutured Laurentian and Baltican margins [130], and which resulted in the emplacement of numerous and frequently voluminous acidic to ultrabasic igneous masses [131,132]. Caledonian ages are widespread across the Caledonian orogenic belt within Scotland, Norway and east Greenland e.g., [121,133–135], albeit with varying geographical prevalence. For example, Caledonian intrusions form only a minor component within the East Greenland fold belt, whilst granitoid masses of comparable age are common across the Grampian, Northern Highland and Southern Upland terranes of Scotland, including Shetland (Figure 7). In Scandinavia, Caledonian intrusions are recorded from the Norwegian Caledonides, although these are largely distal from the central North Sea in the upper and uppermost allochthons from Mid Norway and Finnmark. Published Caledonian-age dates from south-western Norway are limited to the Hardangerfjord and Lindås nappes between Karmøy and Fensfjorden, and the Jotun Nappe in the eastern reaches of Sognefjord [133,136,137]. The relatively small number of zircons that can be attributed to the Caledonian orogenic cycle could therefore be reconciled with either a Scottish or Norwegian provenance, or indeed East Greenland, although that is less likely when considering previously published palaeogeographic reconstructions. Although Andrews et al. [138] considered that rivers with a catchment in East Greenland may have extended into the southern Viking Graben, they also acknowledged that the East Shetland Platform (ESP) may have been an alternative source area. As the latter would be consistent with Preston et al. [139] who demonstrated that Triassic sandstones of the Beryl Embayment (location shown in Figure 7) were predominantly sourced from the ORS of the ESP, direct sourcing of Skagerrak Formation sandstones from a considerably more distal source in Greenland seems the less likely option.

The zircon age data, therefore, indicate that at the base of the Joanne Sandstone Member, there was a marked reduction in the supply of sediment that originated in Scotland. This scenario is consistent with the palaeogeographic maps and facies distributions proposed by McKie and Audretsch [11], McKie et al. [12] and Gray et al. [9], in which Scottish-derived sediment transport systems were more extensive in the earlier parts of the Triassic and were subsequently replaced by detritus shed from southern Scandinavia. However, it is important to recognise that zircons are capable of extensive recycling owing to their mechanical and chemical stability, and hence the Archaean component in the Smith



Bank and Judy zircon populations may not necessarily indicate first-cycle supply from Scottish basement terranes.

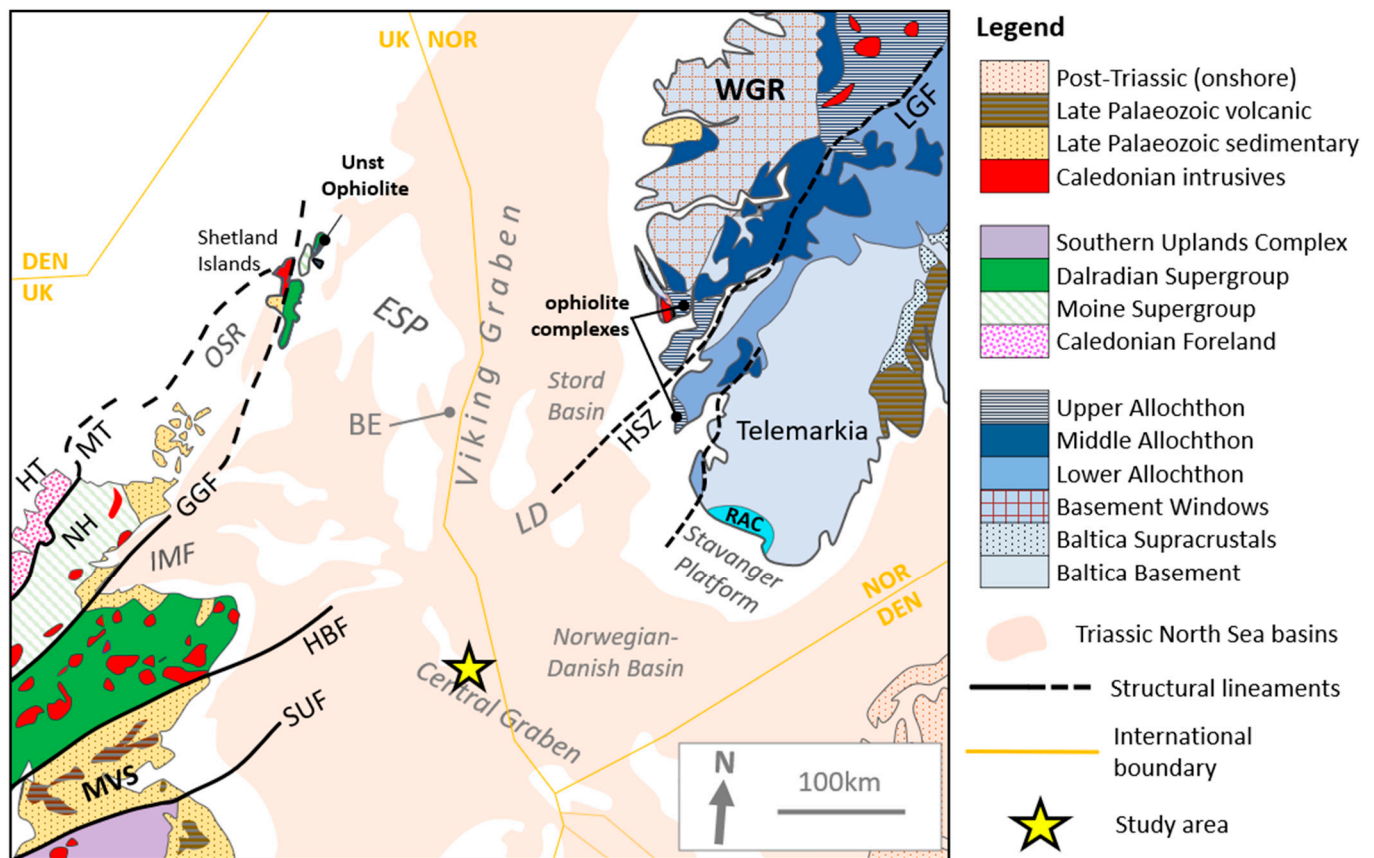


**Figure 7.** Geological summary map of the geological units exposed on the landmasses of Scotland and SW Scandinavia with the location of Triassic basins and structural features discussed in this paper. Abbreviations: BE, Beryl Embayment; ESP, East Shetland Platform; GGF, Great Glen Fault; HSZ, Hardangerfjord Shear Zone; HBF, Highland Boundary Fault; HT, Hebridean Terrane; IMF, Inner Moray Firth; LD, Ling Depression; LGF, Lærdal–Gjende Fault Complex; MT, Moine Thrust; MVS, Midland Valley of Scotland; NH, Northern Highland Terrane; OSR, Orkney–Shetland Ridge; RAC, Rogaland Anorthosite Complex; SUF, Southern Uplands Fault; WGR, Western Gneiss Region. Based on Corfu and Andersen [140], Goldsmith et al. [33], and Holdsworth et al. [97].

## 6.2. Apatite

Interpretation of the detrital apatite age data is necessarily less well-founded than with the zircons, since there is a scarcity of data to compare with the observations in the current study. Nevertheless, a number of conclusions can be drawn, the most fundamental being that the contrast between the Joanne Sandstone Member and older sandstones confirms the zircon evidence for a switch in sediment supply systems. The apatites obtained from the Joanne Sandstone Member are predominantly of Caledonian age, with little representation of the mid-Proterozoic that is so abundant in the zircon spectra. The most likely explanation is that the source areas that provided the mid-Proterozoic zircons (either crystalline basement or recycled from metasediments in the Caledonian Nappes) were subjected to relatively low-temperature metamorphism that caused diffusion of Pb and dissolution-precipitation during the Caledonian orogenic cycle. This scenario is compatible with the known geological framework of southern and western Norway.

In the Bunter Sandstone Member and Judy Sandstone Member, there is also a mismatch between the zircon and apatite spectra. The Caledonian peaks broadly correlate, but the majority of the mid-Proterozoic zircons post-date the Palaeoproterozoic-Mesozoic apatites,

and the Archaean group that is characteristic of the zircon population is either poorly represented or entirely absent. The explanation for the absence of mid-Proterozoic apatites corresponding to the zircons as proposed above for the Joanne Sandstone Member could also apply to the Bunter and Judy samples and would be again compatible with the geological framework of northern Scotland. The origin of the older apatite group, however, requires another explanation, since it evidently points towards a source that was unaffected by Caledonian thermal events.

One explanation for this group of apatites is that they were derived from the Lewisian Complex that supplied the Archaean zircons, since this region was affected by at least two Laxfordian tectonothermal events, one from 1910 Ma to 1850 Ma and another around 1750–1650 Ma [141]. The same explanation has been applied to the Stoer Group, which shows a closely comparable group of apatites in the 1500–1900 Ma age range [63,142], in association with zircons at ca. 2750 Ma. O’Sullivan et al. [63] note that the Laxfordian event is poorly represented in the zircon U-Pb record even though most apatite in the Stoer Group yields Laxfordian U-Pb ages. An alternative origin is that these apatites represent input from Greenland, since a comparable U-Pb apatite-based study from SW Greenland [143] records thermal overprinting within this area at  $1826 \pm 9$  Ma, which is an excellent match with the peak abundance at ca. 1825 Ma in sample MK-2.

### 6.3. Conclusions

The change in provenance at the base of the Joanne Sandstone Member identified on the basis of conventional heavy mineral data [16] is verified by the zircon and apatite data described in this paper (Figure 8). The key changes are (i) the abundance of Archaean zircons in the Bunter Sandstone Member and Judy Sandstone Member, and their marked decrease in the Joanne Sandstone Member, and (ii) the abundance of Meso- and Palaeoproterozoic apatites in the Bunter Sandstone Member and Judy Sandstone Member, and their virtually complete absence in the Joanne Sandstone Member. These results provide strong support for a reorganisation of sediment transport systems between the Judy and Joanne sandstones in the Culzean area.

The combined apatite and zircon data suggest that the source region for the Bunter Sandstone Member and the Judy Sandstone Member comprises Moian-Dalradian metasediments affected by tectonothermal events associated with the Caledonian orogenic cycle, in conjunction with a Palaeoproterozoic-Archaean source originating outside of this deformation zone. The only feasible Palaeoproterozoic-Archaean foreland areas are the Archaean complexes of NW Scotland (Lewisian Gneiss) and central Greenland (Rae Craton). However, both of these regions were separated from the central North Sea by topographic highs and proto-Atlantic rift basins, respectively [144,145], suggesting that the sediment cannot have been input directly from either area, and that recycling is the most likely possibility. This is supported by the textural evidence from detrital apatite morphologies [15,16], although the observed high apatite roundness might alternatively be attributable to processes operating during the early Triassic depositional cycle. Acquisition of further constraints on the location and nature of the Scottish source is a focus of further studies into Triassic sandstone provenance in the central North Sea region.

In the Joanne Sandstone Member, the association of predominantly Caledonian age apatites with zircons dominated by mid-Proterozoic ages is compatible with the known geological framework of southern and western Norway, where the lithologies that sourced the mid-Proterozoic zircons (either crystalline basement or recycled from metasediments in the Caledonian Nappes) were subjected to relatively low-temperature metamorphism during the Caledonian orogenic cycle and therefore yielding early Palaeozoic apatites. The low degree of textural maturity associated with the detrital apatite, together with the unimodal Caledonian age grouping, indicates a strong first-cycle component. Combined with the common presence of chrome spinel, the Hardangerfjord and surrounding areas of SW Norway would seem a strong candidate source area considering that now-isolated remnants of ophiolite- and granitoid mass-bearing Caledonian allochthons indicate that

widespread erosion of these nappes and Proterozoic metasedimentary units has occurred across this area that was subjected to Late Triassic exhumation [44]. Support for such an interpretation is strengthened by the consideration that any river paths influenced by the SW-NE-trending Hardangerfjord Shear Zone (Figure 7), which may have experienced Triassic exhumation rates of  $>100 \text{ m Myr}^{-1}$  in its footwall [43], would likely enter the central North Sea via the Ling Depression area in a manner consistent with the Joanne depositional model of Gray et al. [9]. However, a shift to a predominantly Fennoscandian-sourced system was not necessarily the result of hinterland tectonics, and alternative causes such as wetting of the hinterland climate during the Late Triassic (cf. McKie [5]), and/or more easterly sub-basins such as the Stord and Norwegian-Danish basins potentially impeding long-distance spill to a greater degree during the Early-Middle Triassic, should also be considered.

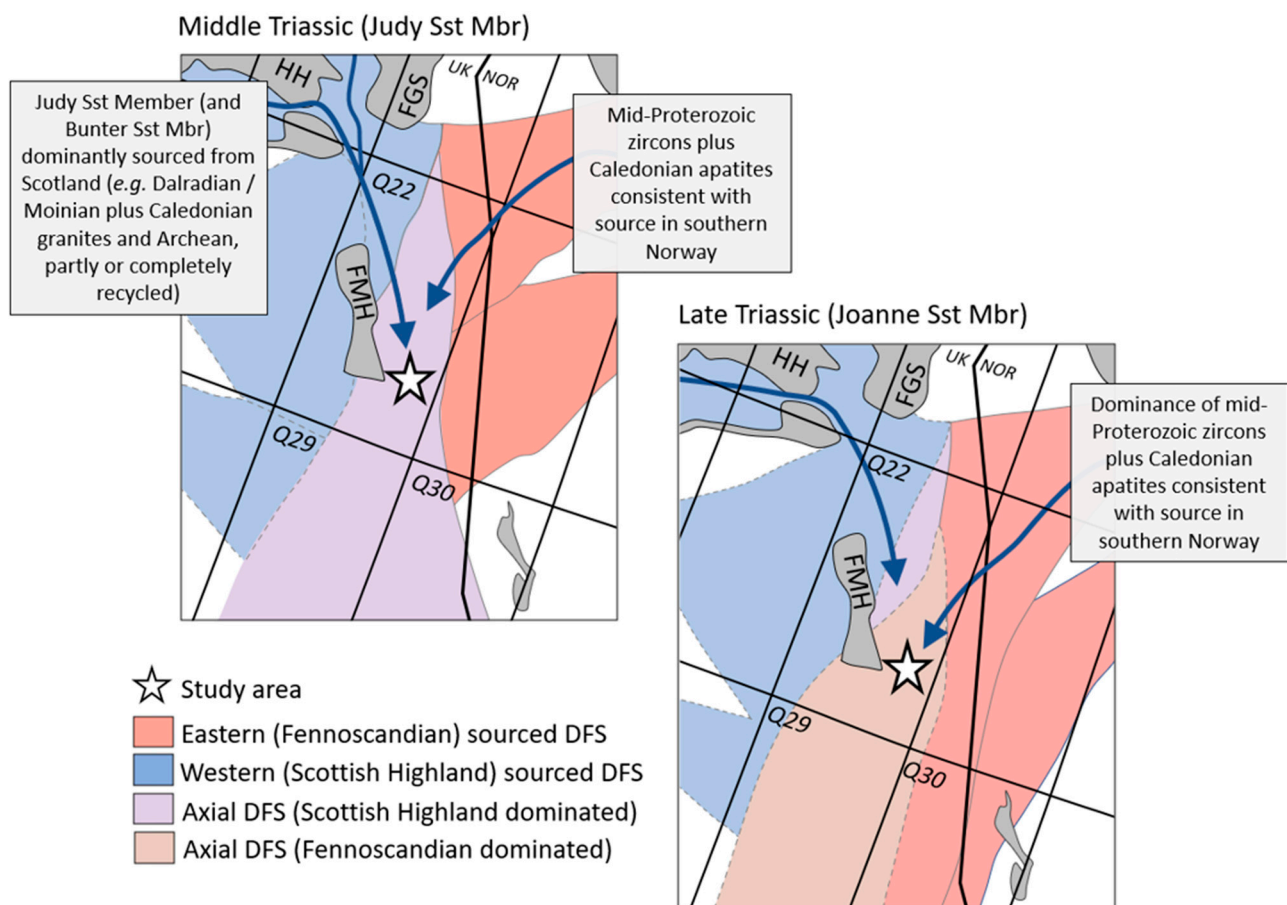


**Figure 8.** Inferred transport routes and likely source lithologies for Judy and Joanne sandstones in the Culzean-Marnock study area based on zircon and apatite data, overlain onto the schematic Middle and Late Triassic depositional systems described by Gray et al. [9].

The application of detrital zircon and apatite geochronology and trace element analysis, in combination with existing conventional and textural heavy mineral studies, has provided detailed information on sediment source areas, lithologies and geochronological histories for sandstones from which a considerable amount of provenance information has been lost through burial diagenetic processes. It may be possible to obtain further constraints using the other ultrastable mineral components (rutile, tourmaline, chrome spinel) in future studies.

**Supplementary Materials:** The following supporting information can be downloaded at: <https://www.mdpi.com/article/10.3390/geosciences13010013/s1>, Table S1: Culzean-Marnock zircon U-Pb data. Table S2: Culzean-Marnock apatite U-Pb data cPb uncorrected. Table S3: Culzean-Marnock apatite trace element data.

**Author Contributions:** Conceptualization, I.P.G., A.H. and A.M.; methodology, I.P.G., A.M. and D.F.; writing—original draft preparation, I.P.G. and A.M.; writing—review and editing, I.P.G., A.M., D.F. and A.H. All authors have read and agreed to the published version of the manuscript.

**Funding:** This research was funded by a grant from the Triassic JIP Phase 2 award to A.H.

**Acknowledgments:** The Triassic Phase 2 Consortium members, BP, Total, JX Nippon and Cairn Energy are gratefully acknowledged for their support of this work. Thanks also go to Mick Pointon (CASP), who undertook the common Pb correction for apatite analyses using the  $^{207}\text{Pb}$  method.

**Conflicts of Interest:** The authors declare no conflict of interest.

## References

1. Pooler, J.; Amory, M. A subsurface perspective on ETAP—an integrated development of seven North Sea fields. In *Petroleum Geology of Northwest Europe: Proceedings of the 5th Conference*; Fleet, A.J., Boldy, S.A.R., Eds.; Geological Society: London, UK, 1999; pp. 993–1006.
2. Archer, S.; Ward, S.; Menad, S.; Shahim, I.; Grant, N.; Sloan, H.; Cole, A. The Jasmine discovery, Central North Sea, UKCS. In *Petroleum Geology: From Mature Basins to New Frontiers: Proceedings of the 7th Petroleum Geology Conference*; Vining, B.A., Pickering, S.C., Eds.; Geological Society: London, UK, 2010; pp. 225–243.
3. Hodgson, N.A.; Farnsworth, J.; Fraser, A.J. Salt-related tectonics, sedimentation and hydrocarbon plays in the Central Graben, North Sea, UKCS. In *Geological Insights for the Next Decade*; Hardman, R.F.P., Ed.; Geological Society: London, UK, 1992; Special Publications; Volume 67, pp. 31–63.
4. Smith, R.I.; Hodgson, N.; Fulton, M. Salt control on Triassic reservoir distribution, UKCS Central North Sea. In *Petroleum Geology of Northwest Europe: Proceedings of the 4th Conference*; Parker, J.R., Ed.; Geological Society: London, UK, 1993; pp. 547–557.
5. McKie, T. Climatic and tectonic controls on Triassic dryland terminal fluvial system architecture, Central North Sea. In *Depositional Systems to Sedimentary Successions on the Norwegian Continental Margin*; Martinus, A.W., Ravnås, R., Howell, J.A., Steel, R.J., Wonham, J.P., Eds.; Wiley: Blackwell, UK, 2014; pp. 19–57.
6. Stricker, S.; Jones, S.J.; Sathar, S.; Bowen, L.; Oxtoby, N. Exceptional reservoir quality in HPHT reservoir settings: Examples from the Skagerrak Formation of the Heron Cluster, North Sea, UK. *Mar. Pet. Geol.* **2016**, *77*, 198–215. [[CrossRef](#)]
7. Cui, Y.; Jones, S.J.; Saville, C.; Stricker, S.; Wang, G.; Tang, L.; Fan, X.; Chen, J. The role played by carbonate cementation in controlling reservoir quality of the Triassic Skagerrak Formation, Norway. *Mar. Pet. Geol.* **2017**, *85*, 316–331. [[CrossRef](#)]
8. Akpokodje, M.; Melvin, A.; Churchill, J.; Burns, S.; Morris, J.; Kape, S.; Wakefield, M.; Ameerli, R. Regional study of controls on reservoir quality in the Triassic Skagerrak Formation of the Central North Sea. In *Petroleum Geology of NW Europe: 50 Years of Learning: Proceedings of the 8th Petroleum Geology Conference*; Bowman, M., Levell, B., Eds.; Geological Society: London, UK, 2018; pp. 125–146.
9. Gray, E.; Hartley, A.; Howell, J. The influence of stratigraphy and facies distribution on reservoir quality and production performance in the Triassic Skagerrak Formation of the UK and Norwegian Central North Sea. In *Cross-Border Themes in Petroleum Geology I: The North Sea*; Patruno, S., Archer, S.G., Chiarella, D., Howell, J.A., Jackson, C.A.L., Kombrink, H., Eds.; Geological Society: London, UK, 2020; Special Publications; Volume 494.
10. Smyth, H.R.; Morton, A.C.; Richardson, N.; Scott, R.A. Sediment provenance studies in hydrocarbon exploration and production: An introduction. In *Sediment Provenance Studies in Hydrocarbon Exploration and Production*; Scott, R.A., Smyth, H.R., Morton, A.C., Richardson, N., Eds.; Geological Society: London, UK, 2015; Special Publication; Volume 386, pp. 1–6.
11. McKie, T. and Audretsch, P. Depositional and structural controls on Triassic reservoir performance in the Heron Cluster, ETAP, Central North Sea. In *Petroleum Geology: North-West Europe and Global Perspectives: Proceedings of the 6th Petroleum Geology Conference*; Doré, A.G., Vining, B.A., Eds.; Geological Society: London, UK, 2005; pp. 285–298.
12. McKie, T.; Jolley, S.J.; Kristensen, M.B. Stratigraphic and structural compartmentalization of dryland fluvial reservoirs: Triassic Heron Cluster, Central North Sea. In *Reservoir Compartmentalization*; Jolley, S.J., Fisher, Q.J., Ainsworth, R.B., Vrolijk, P.J., Delisle, S., Eds.; Geological Society: London, UK, 2010; Special Publications; Volume 347, pp. 165–198.
13. Jarsve, E.M.; Maast, T.; Gabrielsen, R.H.; Faleide, J.I.; Nystuen, J.P.; Sassier, C. Seismic stratigraphic subdivision of the Triassic succession in the Central North Sea, integrating seismic reflection and well data. *J. Geol. Soc.* **2014**, *171*, 353–374. [[CrossRef](#)]
14. Jeans, C.V.; Reed, S.J.B.; Xing, M. Heavy mineral stratigraphy in the UK Trias: Western Approaches, onshore England and the Central North Sea. In *Petroleum Geology of Northwest Europe: Proceedings of the 4th Conference*; Parker, J.R., Ed.; Geological Society: London, UK, 1993; pp. 609–624.

15. Mange-Rajetzky, M.A. Subdivision and correlation of monotonous sandstone sequences using high-resolution heavy mineral analysis, a case study: The Triassic of the Central Graben. In *Dating and Correlating Biostratigraphically-Barren Strata*; Dunay, R.E., Hailwood, E., Eds.; Geological Society: London, UK, 1995; Special Publications; Volume 89, pp. 23–30.
16. Mouritzen, C.; Farris, M.A.; Morton, A.; Matthews, S. Integrated Triassic stratigraphy of the greater Culzean area, UK central North Sea. *Pet. Geosci.* **2017**, *24*, 197–207. [[CrossRef](#)]
17. Goldsmith, P.J.; Rich, B.; Standring, J. Triassic correlation and stratigraphy in the South Central Graben, UK North Sea. In *Permian and Triassic Rifting in Northwest Europe*; Boldy, S.A.R., Ed.; Geological Society: London, UK, 1995; Special Publications; Volume 91, pp. 123–143.
18. Burgess, R.; Jolley, D.; Hartley, A. Stratigraphical palynology of the Middle to Late Triassic successions of the Central North Sea. *Pet. Geosci.* **2021**, *128*. [[CrossRef](#)].
19. Hurst, A.; Morton, A. Provenance models: The role of sandstone mineral-chemical stratigraphy. In *Sediment Provenance Studies in Hydrocarbon Exploration and Production*; Scott, R.A., Smyth, H., Morton, A., Richardson, N., Eds.; Geological Society of London: London, UK, 2014; Special Publications; Volume 386, pp. 7–26.
20. Ziegler, P.A. Evolution of the Arctic-North Atlantic and the Western Tethys. *Mem. Am. Assoc. Pet. Geol.* **1988**, *43*, 164–196.
21. McKie, T.; Williams, B. Triassic palaeogeography and fluvial dispersal across the northwest European basins. *Geol. J.* **2009**, *44*, 711–741. [[CrossRef](#)]
22. Ziegler, P.A.; Van Hoorn, B. Evolution of the North Sea rift system. In *Extensional Tectonics and Stratigraphy of the North Atlantic Margins*; Tankard, A.J., Balkwill, H.R., Eds.; Memoir of the American Association of Petroleum Geologists: Tulsa, OK, USA, 1989; Volume 46, pp. 471–500.
23. Penge, J.; Munns, J.W.; Taylor, B.; Windle, T.M.F. Rift-raft tectonics: Examples of gravitational tectonics from the Zechstein basins of northwest Europe. In *Petroleum Geology of Northwest Europe: Proceedings of the 5th Conference*; Fleet, A.J., Boldy, S.A.R., Eds.; Geological Society: London, UK, 1999; pp. 201–213.
24. Cartwright, J.; Stewart, S.; Clark, J. Salt dissolution and salt-related deformation of the Forth Approaches Basin, UK North Sea. *Mar. Pet. Geol.* **2001**, *18*, 757–778. [[CrossRef](#)]
25. Jackson, C.A.L.; Kane, K.E.; Larsen, E. Structural evolution of minibasins on the Utsira High, northern North Sea; implications for Jurassic sediment dispersal and reservoir distribution. *Pet. Geosci.* **2010**, *16*, 105–120. [[CrossRef](#)]
26. Glennie, K.W. Permian and Triassic rifting in northwest Europe. In *Permian and Triassic Rifting in Northwest Europe*; Boldy, S.A.R., Ed.; Geological Society: London, UK, 1995; Special Publications; Volume 91, pp. 1–5.
27. Karlo, J.F.; Van Buchem, F.S.P.; Moen, J.; Milroy, K. Triassic-age salt tectonics of the Central North Sea. Interpretation. *Interpretation* **2014**, *2*, SM19–SM28. [[CrossRef](#)]
28. Roberts, A.M.; Badley, M.E.; Price, J.D.; Huck, I.W. The structural history of a transtensional basin: Inner Moray Firth, NE Scotland. *J. Geol. Soc.* **1990**, *147*, 87–103. [[CrossRef](#)]
29. Badley, M.E.; Price, J.D.; Dahl, C.R.; Agdestein, T. The structural evolution of the north Viking Graben and its bearing upon extensional modes of basin formation (North Sea). *J. Geol. Soc.* **1988**, *145*, 455–472. [[CrossRef](#)]
30. Steel, R.; Ryseth, A. The Triassic—Early Jurassic succession in the northern North Sea: Megasequence stratigraphy and intra-Triassic tectonics. In *Tectonic Events Responsible for Britain's Oil and Gas Reserves*; Hardman, R.F.P., Brooks, J., Eds.; Geological Society: London, UK, 1990; Special Publications; Volume 55, pp. 139–168.
31. Kuznir, N.J.; Park, R.G. The extensional strength of the continental lithosphere: Its dependence on geothermal gradient, crustal composition and thickness. In *Continental Extensional Tectonics*; Coward, M.P., Dewey, J.F., Hancock, P.L., Eds.; Geological Society: London, UK, 1987; Special Publications; Volume 28, pp. 35–52.
32. Fisher, M.J.; Mudge, D.C. Triassic. In *Introduction to the Petroleum Geology of the North Sea*; Glennie, K.W., Ed.; Blackwell Scientific Publications: Oxford, UK, 1990; pp. 191–218.
33. Goldsmith, P.J.; Hudson, G.; van Veen, P. Triassic. In *The Millennium Atlas: Petroleum Geology of the Central and Northern North Sea*; Evans, D., Graham, C., Armour, A., Bathurst, P., Eds.; Geological Society: London, UK, 2003; pp. 123–143.
34. Cameron, T.D.J. Triassic, Permian and Pre-Permian of the Central and Northern North Sea. In *Lithostratigraphic Nomenclature of the UK North Sea*; Knox, R.W.O'B., Cordey, W.G., Eds.; British Geological Survey: Nottingham, UK, 1993; pp. 25–41.
35. Archer, S.G.; McKie, T.; Andrews, S.D.; Wilkins, A.D.; Hutchison, M.; Young-Ziolkowski, N.; Osunde, C.; Matheson, J.; Thackrey, S.; Lang, M.; et al. Triassic mudstones of the Central North Sea: Cross-border characterization, correlation and their palaeoclimatic significance. In *Cross-Border Themes in Petroleum Geology I: The North Sea*; Patruno, S., Archer, S.G., Chiarella, D., Howell, J.A., Jackson, C.A.L., Kombrink, H., Eds.; Geological Society: London, UK, 2020; Special Publications; Volume 494, pp. 333–378.
36. Cohen, K.M.; Finney, S.C.; Gibbard, P.L.; Fan, J.-X. The ICS International Chronostratigraphic Chart. *Epis. J. Int. Geosci.* **2013**, *36*, 199–204. [[CrossRef](#)] [[PubMed](#)]
37. Sellwood, B.W.; Valdes, P.J. Mesozoic climates: General circulation models and the rock record. *Sediment. Geol.* **2006**, *190*, 269–287. [[CrossRef](#)]
38. Ruffell, A.; Simms, M.J.; Wignall, P.B. The Carnian humid episode of the late Triassic: A review. *Geol. Mag.* **2016**, *153*, 271–284. [[CrossRef](#)]
39. Wilkins, A.D.; Hurst, A.; Wilson, M.J.; Archer, S. Palaeo-environment in an ancient low-latitude, arid lacustrine basin with loessite: The Smith Bank Formation (Early Triassic) in the Central North Sea, UK Continental Shelf. *Sedimentology* **2017**, *65*, 335–359. [[CrossRef](#)]

40. Burgess, R.; Jolley, D.; Hartley, A. Palaeoenvironmental reconstruction of Triassic floras from the Central North Sea. *J. Geol. Soc.* **2022**, *179*. [[CrossRef](#)]
41. Hendriks, B.W.H.; Andriessen, P.A.M.; Huigen, Y.D.; Leighton, C.; Redfield, T.F.; Murrell, G.R.; Gallagher, K.; Nielsen, S.B. A fission track data compilation for Fennoscandia. *Nor. Geol. Tidsskr.* **2007**, *87*, 143–155.
42. Holford, S.P.; Green, P.F.; Hillis, R.R.; Underhill, J.R.; Stoker, M.S.; Duddy, I.R. Multiple post-Caledonian exhumation episodes across NW Scotland revealed by apatite fission-track analysis. *J. Geol. Soc.* **2010**, *167*, 675–694. [[CrossRef](#)]
43. Johannessen, K.C.; Kohlmann, F.; Ksienzyk, A.K.; Dunkl, I.; Jacobs, J. Tectonic evolution of the SW Norwegian passive margin based on low-temperature thermochronology from the innermost Hardangerfjord area. *Nor. Geol. Tidsskr.* **2013**, *93*, 243–260.
44. Ksienzyk, A.K.; Dunkl, I.; Jacobs, J.; Fossen, H.; Kohlmann, F. From orogen to passive margin: Constraints from fission track and (U-Th)/He analyses on Mesozoic uplift and fault reactivation in SW Norway. In *New Perspectives on the Caledonides of Scandinavia and Related Areas*; Corfu, F., Gasser, D., Chew, D.M., Eds.; Geological Society: London, UK, 2014; Special Publications; Volume 390, pp. 679–702.
45. Thomson, K.; Underhill, J.R.; Green, P.F.; Bray, R.J.; Gibson, H.J. Evidence from apatite fission track analysis for the post-Devonian burial and exhumation history of the northern Highlands, Scotland. *Mar. Pet. Geol.* **1999**, *16*, 27–39. [[CrossRef](#)]
46. Japsen, P.; Green, P.F.; Chalmers, J.A.; Bonow, J.M. Mountains of southernmost Norway: Uplifted Miocene peneplains and re-exposed Mesozoic surfaces. *J. Geol. Soc.* **2018**, *175*, 721–741. [[CrossRef](#)]
47. Fredin, O.; Viola, G.; Zwingsmann, H.; Sørli, R.; Brønner, M.; Lie, J.; Grandal, E.M.; Müller, A.; Margreth, A.; Vogt, C.; et al. The inheritance of a Mesozoic landscape in western Scandinavia. *Nat. Commun.* **2017**, *8*, 14879. [[CrossRef](#)] [[PubMed](#)]
48. Stricker, S.; Jones, S.J.; Meadows, N.; Bowen, L. Reservoir quality of fluvial sandstone reservoirs in salt-walled mini-basins: An example from the Seagull field, Central Graben, North Sea, UK. *Pet. Sci.* **2018**, *15*, 1–27. [[CrossRef](#)]
49. Racey, A.; Love, M.A.; Bobolecki, R.M.; Walsh, J.N. The use of chemical element analyses in the study of biostratigraphically barren sequences: An example from the Triassic of the central North Sea (UKCS). In *Dating and Correlating Biostratigraphically-Barren Strata*; Dunay, R.E., Hailwood, E., Eds.; Geological Society: London, UK, 1995; Special Publications; Volume 89, pp. 69–105.
50. Rubey, W.W. The size distribution of heavy minerals within a water-lain sandstone. *J. Sediment. Petrol.* **1933**, *3*, 3–29.
51. Baba, J.; Komar, P.D. Settling velocities of irregular grains at low Reynolds numbers. *J. Sediment. Petrol.* **1981**, *51*, 121–128.
52. Garzanti, E.; Andò, S.; Vezzoli, G. Settling equivalence of detrital minerals and grain-size dependence of sediment composition. *Earth Planet. Sci. Lett.* **2008**, *273*, 138–151. [[CrossRef](#)]
53. Pedersen, R.B.; Furnes, H.; Dunning, G.R. Some Norwegian ophiolites reconsidered. *Norges Geologiske Undersøgelse* **1988**, *3*, 80–85.
54. Bluck, B.J. The Highland Boundary Fault and the Highland Border Complex. *Scott. J. Geol.* **2010**, *46*, 113–124. [[CrossRef](#)]
55. Crowley, Q.G.; Strachan, R.A. U–Pb zircon constraints on obduction initiation of the Unst Ophiolite: An oceanic core complex in the Scottish Caledonides? *J. Geol. Soc.* **2015**, *172*, 279–282. [[CrossRef](#)]
56. Breithfeld, H.T.; Hall, R. The eastern Sundaland margin in the latest Cretaceous to Late Eocene: Sediment provenance and depositional setting of the Kuching and Sibuluan zones of Borneo. *Gondwana Res.* **2018**, *63*, 34–64. [[CrossRef](#)]
57. Martin, J.R.; Redfern, J.; Horstwood, M.S.A.; Mory, A.J.; Williams, B.P.J. Detrital zircon age and provenance constraints on late Paleozoic ice-sheet growth and dynamics in Western and Central Australia. *Aust. J. Earth Sci.* **2019**, *66*, 183–207. [[CrossRef](#)]
58. Meinhold, G.; Bassis, A.; Hinderer, M.; Lewin, A.; Berndt, J. Detrital zircon provenance of north Gondwana Palaeozoic sandstones from Saudi Arabia. *Geol. Mag.* **2021**, *158*, 442–458. [[CrossRef](#)]
59. Sláma, J.; Walderhaug, O.; Fonneland, H.; Kosler, J.; Pedersen, R.B. Provenance of Neoproterozoic to upper Cretaceous sedimentary rocks, eastern Greenland: Implications for recognizing the sources of sediments in the Norwegian Sea. *Sediment. Geol.* **2011**, *238*, 254–267. [[CrossRef](#)]
60. Sharman, G.R.; Graham, S.A.; Grove, M.; Kimbrough, D.L.; Wright, J.E. Detrital zircon provenance of the Late Cretaceous–Eocene California forearc: Influence of Laramide low-angle subduction on sediment dispersal and palaeogeography. *Bull. Geol. Soc. Am.* **2015**, *127*, 38–60. [[CrossRef](#)]
61. Morton, A.C.; Claoué-Long, J.C.; Hallsworth, C.R. Zircon age and heavy mineral constraints on provenance of North Sea Carboniferous sandstones. *Mar. Pet. Geol.* **2001**, *18*, 319–337. [[CrossRef](#)]
62. Lundmark, A.M.; Bue, E.P.; Gabrielsen, R.H.; Flaath, K.; Strand, T.; Ohm, S.E. Provenance of late Palaeozoic terrestrial sediments on the northern flank of the Mid North Sea High: Detrital zircon geochronology and rutile geochemical constraints. In *Sediment Provenance Studies in Hydrocarbon Exploration and Production*; Scott, R.A., Smyth, H.R., Morton, A.C., Richardson, N., Eds.; Geological Society: London, UK, 2014; Special Publications; Volume 386, pp. 243–259.
63. O’Sullivan, G.; Chew, D.; Kenny, G.; Henrichs, I.; Mulligan, D. The trace element composition of apatite and its application to detrital provenance studies. *Earth-Sci. Rev.* **2020**, *201*, 103044. [[CrossRef](#)]
64. Cherniak, D.J. Diffusion in accessory minerals: Zircon, titanite, apatite, monazite and xenotime. *Rev. Mineral. Geochem.* **2010**, *72*, 827–869. [[CrossRef](#)]
65. Harlov, D.E. Apatite: A fingerprint for metasomatic processes. *Elements* **2015**, *11*, 171–176. [[CrossRef](#)]
66. Greig, I.P. Heavy Mineral Stratigraphy and Provenance of Triassic Sediments of the Central North Sea and Moray Firth. Ph.D. Thesis, University of Aberdeen, Aberdeen, UK, 2021.
67. Morton, A.C.; Hallsworth, C.R. Identifying provenance-specific features of detrital heavy mineral assemblages in sandstones. *Sediment. Geol.* **1994**, *90*, 241–256. [[CrossRef](#)]

68. Morton, A.C.; Hallsworth, C.R.; Kunka, J.; Laws, E.; Payne, S.; Walder, D. Heavy mineral stratigraphy of the Clair Group (Devonian) in the Clair Field, west of Shetland, UK. In *Application of Modern Stratigraphic Techniques: Theory and Case Histories*; Ratcliffe, K.T., Zaitlin, B.A., Eds.; SEPM: Tulsa, OK, USA, 2010; Special Publications; Volume 94, pp. 183–199.
69. Gerdes, A.; Zeh, A. Combined U-Pb and Hf isotope LA-(MC-)ICP-MS analyses of detrital zircons: Comparison with SHRIMP and new constraints for the provenance and age of an Armorican metasediment in Central Germany. *Earth Planet. Sci. Lett.* **2006**, *249*, 47–61. [CrossRef]
70. Frei, D.; Gerdes, A. Precise and accurate in situ U-Pb dating of zircon with high sample throughput by automated LA-SF-ICP-MS. *Chem. Geol.* **2009**, *261*, 261–270. [CrossRef]
71. Sláma, J.; Košler, J.; Condon, D.J.; Crowley, J.L.; Gerdes, A.; Hanchar, J.M.; Horstwood, M.S.A.; Morris, G.A.; Nasdala, L.; Norberg, N.; et al. Plešovice zircon—a new natural reference material for U-Pb and Hf isotopic microanalysis. *Chem. Geol.* **2008**, *249*, 1–35. [CrossRef]
72. Nasdala, L.; Hofmeister, W.; Norberg, N.; Martinson, J.M.; Corfu, F.; Dörr, W.; Kamo, S.L.; Kennedy, A.K.; Kronz, A.; Reiners, P.W.; et al. Zircon M257—a homogeneous natural reference material for the ion microprobe U-Pb analysis of zircon. *Geostand. Geoanal. Res.* **2008**, *32*, 247–265. [CrossRef]
73. Mattinson, J.M. Analysis of the relative decay constants of <sup>235</sup>U and <sup>238</sup>U by multistep CA-TIMS measurements of closed-system natural zircon samples. *Chem. Geol.* **2010**, *275*, 186–198. [CrossRef]
74. Ludwig, K. *Isoplot/Ex Version 3: A Geochronological Toolkit for Microsoft Excel*; Geochronology Centre: Berkeley, UK, 2003.
75. Sircombe, K.N. AgeDisplay: An EXCEL workbook to evaluate and display univariate geochronological data using binned frequency histograms and probability density distributions. *Comput. Geosci.* **2004**, *30*, 21–31. [CrossRef]
76. Wiedenbeck, M.; Alle, P.; Corfu, F.; Griffin, W.L.; Meier, M.; Oberli, F.; Quadt, A.V.; Roddick, J.C.; Spiegel, W. Three natural zircon standards for U-Th-Pb, Lu-Hf, trace element and REE analyses. *Geostand. Newsl.* **1995**, *19*, 1–23. [CrossRef]
77. Jackson, S.E.; Pearson, N.J.; Griffin, W.L.; Belousova, E.A. The application of laser ablation-inductively coupled plasma-mass spectrometry to in situ U-Pb zircon geochronology. *Chem. Geol.* **2004**, *211*, 47–69. [CrossRef]
78. Stacey, J.S.; Kramers, J.D. Approximation of terrestrial lead isotope evolution by a two-stage model. *Earth Planet. Sci. Lett.* **1975**, *26*, 207–221. [CrossRef]
79. Thomson, S.N.; Gehrels, G.E.; Ruiz, J.; Buchwaldt, R. Routine low-damage U-Pb dating using laser ablation-multicollector-ICPMS. *Geochem. Geophys. Geosyst.* **2012**, *13*, Q0AA21. [CrossRef]
80. Cochrane, R.; Spikings, R.A.; Chew, D.; Wotzlaw, J.F.; Chiaradia, M.; Tyrrell, S.; Schaltegger, U.; Van der Lelij, R. High temperature (>350 °C) thermochronology and mechanisms of Pb loss in apatite. *Geochim. Cosmochim. Acta* **2014**, *127*, 39–56. [CrossRef]
81. Chew, D.M.; Sylvester, P.J.; Tubrett, M.N. U-Pb and Th-Pb dating of apatite by LA-ICPMS. *Chem. Geol.* **2011**, *280*, 200–216. [CrossRef]
82. Jochum, K.P.; Nehring, F. BCR-2: GeoRem Preferred Values. GeoRem, 2006; 11/2006. Available online: <http://georem.mpch-mainz.gwdg.de> (accessed on 4 November 2019).
83. Jochum, K.P.; Nehring, F. BHVO: GeoRem Preferred Values. GeoRem, 2006; 11/2006. Available online: <http://georem.mpch-mainz.gwdg.de> (accessed on 4 November 2019).
84. Jochum, K.P.; Nehring, F. NIST610: GeoRem Preferred Values. GeoRem, 2006; 11/2006. Available online: <http://georem.mpch-mainz.gwdg.de> (accessed on 4 November 2019).
85. Fleischer, M.; Altschuler, Z.S. The lanthanides and yttrium in minerals of the apatite group—an analysis of the available data. *Neues Jahrb. Mineral. Mon.* **1986**, *10*, 467–480.
86. Morton, A.C.; Yaxley, G. Detrital apatite geochemistry and its application in provenance studies. In *Sediment Provenance and Petrogenesis: Perspectives from Petrography and Geochemistry*; Arribas, J., Critelli, S., Johnsson, M.J., Eds.; Special Paper 420; Geological Society of America: Boulder, CO, USA, 2007; pp. 319–344.
87. Belousova, E.A.; Griffin, W.L.; O'Reilly, S.Y.; Fisher, N.I. Apatite as an indicator mineral for mineral exploration: Trace-element compositions and their relationship to host rock type. *J. Geochem. Explor.* **2002**, *76*, 45–69. [CrossRef]
88. O'Sullivan, G.; Chew, D.; Morton, A.; Mark, C.; Henrichs, I. Integrated apatite geochronology and geochemistry in sedimentary provenance analysis. *Geochem. Geophys. Geosyst.* **2018**, *19*, 1309–1326. [CrossRef]
89. Friend, C.R.L.; Kinny, P.D. New evidence for protolith ages of Lewisian granulites, northwest Scotland. *Geology* **1995**, *23*, 1027–1030. [CrossRef]
90. Cawood, P.A.; Nemchin, A.A.; Smith, M.; Loewy, S. Source of the Dalradian Supergroup constrained by U-Pb dating of detrital zircon and implications for the East Laurentian margin. *J. Geol. Soc.* **2003**, *160*, 231–246. [CrossRef]
91. Bingen, B.; Solli, A. Geochronology of magmatism in the Caledonian and Sveconorwegian belts of Baltica: Synopsis for detrital zircon provenance studies. *Nor. Geol. Tidsskr.* **2009**, *89*, 267–290.
92. Cartwright, T.; Fitches, W.R.; O'Hara, M.J.; Barnicoat, A.C.; O'Hara, S. Archaean supracrustal rocks from the Lewisian near Stoer, Sutherland. *Scott. J. Geol.* **1985**, *21*, 187–196. [CrossRef]
93. Park, R.G.; Stewart, A.D.; Wright, D.T. The Hebridean Terrane. In *The Geology of Scotland*; Trewin, N.H., Ed.; Geological Society: London, UK, 2003; pp. 45–61.
94. Ramsay, J.G. Moine-Lewisian relations at Glenelg, Inverness-shire. *Q. J. Geol. Soc. Lond.* **1957**, *113*, 487–524. [CrossRef]

95. Mendum, J.R.; Noble, S.R. Mid-Devonian sinistral transpressional movements on the Great Glen Fault: The rise of the Rosemarkie Inlier and the Acadian event in Scotland. In *Continental Tectonics and Mountain Building: The Legacy of Peach and Horne*; Law, R.D., Butler, R.W.H., Holdsworth, R.E., Krabbendam, M., Strachan, R.E., Eds.; Geological Society: London, UK, 2010; Special Publications; Volume 335, pp. 161–187.
96. Kinny, P.D.; Strachan, R.A.; Fowler, M.; Clark, C.; Davis, S.; Jahn, I.; Taylor, R.J.M.; Holdsworth, R.E.; Dempsey, E. The Neoproterozoic Uyea Gneiss Complex, Shetland: An onshore fragment of the Rae Craton on the European plate. *J. Geol. Soc.* **2019**, *164*, 541–551. [[CrossRef](#)]
97. Holdsworth, R.E.; Morton, A.C.; Frei, D.; Gerdes, A.; Strachan, R.A.; Dempsey, E.; Warren, C.; Whitham, A. The nature and significance of the Faroe-Shetland Terrane: Linking Archaean basement blocks across the North Atlantic. *Precambrian Res.* **2019**, *321*, 154–171. [[CrossRef](#)]
98. Kolb, J. Structure of the Palaeoproterozoic Nagssugtoqidian Orogen, South-East Greenland: Model for the tectonic evolution. *Precambrian Res.* **2014**, *255*, 809–822. [[CrossRef](#)]
99. Lebrun, E.; Árting, T.B.; Kolb, J.; Fiorentini, M.; Kokfelt, T.; Johannesen, A.B.; Maas, R.; Thébaud, N.; Martin, L.A.J.; Murphy, R.C. Genesis of the Paleoproterozoic Ammassalik Intrusive Complex, south-east Greenland. *Precambrian Res.* **2018**, *315*, 19–44. [[CrossRef](#)]
100. Love, G.J.; Kinny, P.D.; Friend, C.R.L. Timing of magmatism and metamorphism in the Guinard Bay area of the Lewisian Gneiss Complex: Comparisons with the Assynt Terrane and implications for terrane accretion. *Contrib. Mineral. Petrol.* **2004**, *146*, 620–636. [[CrossRef](#)]
101. Friend, C.R.L.; Nutman, A.P.; McGregor, V.R. Late-Archaean tectonics in the Faeringehavn-Tre Brødre area, south of Buksefjorden, southern West Greenland. *J. Geol. Soc.* **1987**, *144*, 369–376. [[CrossRef](#)]
102. Schmidt, A.S.; Morton, A.C.; Nichols, G.J.; Fanning, C.M. Interplay of proximal and distal sources in Devonian–Carboniferous sandstones of the Clair Basin, West of Shetland, revealed by detrital zircon U–Pb ages. *J. Geol. Soc.* **2012**, *169*, 691–702. [[CrossRef](#)]
103. Sałnowski, A.S. Palaeogeographic Implications of Heavy Mineral and Detrital Zircon Provenance of Devonian–Carboniferous Sedimentary Rocks in the North Atlantic Region. Ph.D. Thesis, Royal Holloway, University of London, London, UK, 2014.
104. Cawood, P.A.; Nemchin, A.A.; Strachan, R.; Prave, A.; Krabbendam, M. Sedimentary basin and detrital zircon record along East Laurentia and Baltica during assembly and breakup of Rodinia. *J. Geol. Soc.* **2007**, *164*, 257–275. [[CrossRef](#)]
105. Johnson, T.E.; Kirkland, C.L.; Reddy, S.M.; Evans, N.J.; McDonald, B.J. The source of Dalradian detritus in the Buchan Block, NE Scotland: Application of new tools to detrital datasets. *J. Geol. Soc.* **2016**, *173*, 773–782. [[CrossRef](#)]
106. Kinnaird, T.C.; Prave, A.R.; Kirkland, C.L.; Horstwood, M.; Parrish, R.; Batchelor, R.A. The late Mesoproterozoic–early Neoproterozoic tectonostratigraphic evolution of NW Scotland: The Torridonian revisited. *J. Geol. Soc.* **2007**, *173*, 773–782. [[CrossRef](#)]
107. Dawes, P.R. The bedrock geology under the Inland Ice: The next major challenge for Greenland mapping. *Geol. Surv. Den. Greenl. Bull.* **2009**, *17*, 57–60. [[CrossRef](#)]
108. Bergh, S.G.; Kullerud, K.; Corfu, F.; Armitage, P.E.B.; Davidsen, B.; Johansen, H.W.; Pettersen, T.; Knudsen, S. Low-grade sedimentary rocks on Vanna, North Norway: A new occurrence of a Palaeoproterozoic (2.4–2.2 Ga) cover succession in northern Fennoscandia. *Nor. Geol. Tidsskr.* **2007**, *87*, 301–318.
109. Beyer, E.E.; Brueckner, H.K.; Griffin, W.L.; O’Reilly, S.Y. Laurentian provenance of Archean mantle fragments in the Proterozoic Baltic crust of the Norwegian Caledonides. *J. Petrol.* **2012**, *53*, 1357–1383. [[CrossRef](#)]
110. Sláma, J.; Pedersen, R.B. Zircon provenance of SW Caledonian phyllites reveals a distant Timanian sediment source. *J. Geol. Soc.* **2015**, *172*, 465–478. [[CrossRef](#)]
111. Slagstad, T.; Kirkland, C.L. The use of detrital zircon data in terrane analysis: A non-unique answer to provenance and tectonostratigraphic position in the Scandinavian Caledonides. *Lithosphere* **2017**, *9*, 1002–1011. [[CrossRef](#)]
112. Lamminen, J. Provenance and correlation of sediments in Telemark, South Norway: Status of the Lifjell Group and implications for early Sveconorwegian fault tectonics. *Nor. Geol. Tidsskr.* **2011**, *91*, 57–75.
113. Lundmark, A.M.; Lamminen, J. The provenance and setting of the Mesoproterozoic Dala Sandstone, western Sweden, and paleogeographic implications for southwestern Fennoscandia. *Precambrian Res.* **2016**, *275*, 197–208. [[CrossRef](#)]
114. Åhäll, K.; Gower, C.F. The Gothian and Labradorian orogens: Variations in accretionary tectonism along a late Paleoproterozoic Laurentia–Baltica margin. *GFF* **1997**, *119*, 181–191. [[CrossRef](#)]
115. Gower, C.F.; Kamo, S.L.; Kwok, K.; Krogh, T.E. Proterozoic southward accretion and Grenvillian orogenesis in the interior Grenville Province in eastern Labrador: Evidence from U–Pb geochronological investigations. *Precambrian Res.* **2008**, *165*, 61–95. [[CrossRef](#)]
116. Connelly, J.N.; Åhäll, K. The Mesoproterozoic cratonization of Baltica—new age constraints from SW Sweden. In *Precambrian Crustal Evolution in the North Atlantic Region*; Brewer, T.S., Ed.; Geological Society: London, UK, 1996; Special Publications; Volume 112, pp. 261–273.
117. Kirkland, C.L.; Daly, J.S.; Whitehouse, M.J. Provenance and terrane evolution of the Kalak Nappe Complex, Norwegian Caledonides: Implications for Neoproterozoic paleogeography and tectonics. *J. Geol.* **2007**, *115*, 21–41. [[CrossRef](#)]
118. Krabbendam, M.; Prave, T.; Cheer, D. A fluvial origin for the Neoproterozoic Morar Group, NW Scotland; implications for Torridon–Morar Group correlation and the Grenville Orogen foreland basin. *J. Geol. Soc.* **2008**, *165*, 379–394. [[CrossRef](#)]



119. Cawood, P.A.; Strachan, R.A.; Merle, R.E.; Millar, I.L.; Loewy, S.L.; Dalziel, I.W.D.; Kinny, P.D.; Jourdan, F.; Nemchin, A.A.; Connelly, J.N. Neoproterozoic to early Paleozoic extensional and compressional history of East Laurentian margin sequences: The Moine Supergroup, Scottish Caledonides. *Bull. Geol. Soc. Am.* **2015**, *127*, 349–371. [[CrossRef](#)]
120. Strachan, R.A.; Nutman, A.P.; Friderichsen, J.D. SHRIMP U-Pb geochronology and metamorphic history of the Smallefjord sequence, NE Greenland Caledonides. *J. Geol. Soc.* **1995**, *152*, 779–784. [[CrossRef](#)]
121. Watt, G.R.; Kinny, P.D.; Friderichsen, J.D. U-Pb geochronology of Neoproterozoic and Caledonian tectonothermal events in the East Greenland Caledonides. *J. Geol. Soc.* **2000**, *157*, 1031–1048. [[CrossRef](#)]
122. Roberts, N.M.W.; Slagstad, T. Continental growth and reworking on the edge of the Columbia and Rodinia supercontinents; 1.86–0.9 Ga accretionary orogeny in southwest Fennoscandia. *Int. Geol. Rev.* **2015**, *57*, 1582–1606. [[CrossRef](#)]
123. Bingen, B.; Skår, Ø.; Marker, M.; Sigmond, E.M.O.; Nordgulen, Ø.; Ragnhildstveit, J.; Mansfeld, J.; Tucker, R.D.; Liégeois, J. Timing of continental building in the Sveconorwegian orogen, SW Scandinavia. *Nor. Geol. Tidsskr.* **2005**, *85*, 87–105.
124. Banks, C.J.; Smith, M.; Winchester, J.A.; Horstwood, M.S.A.; Noble, S.R. Ottley Provenance of intra-Rodinian basin-fills: The lower Dalradian Supergroup, Scotland. *Precamb. Res.* **2007**, *153*, 46–64. [[CrossRef](#)]
125. Slagstad, T.; Roberts, N.M.W.; Kulakov, E. Linking orogenesis across a supercontinent; the Grenvillian and Sveconorwegian margins on Rodinia. *Gondwana Res.* **2017**, *44*, 109–115. [[CrossRef](#)]
126. Moecher, D.P.; Samson, S.D. Differential zircon fertility of source terranes and natural bias in the detrital zircon record: Implications for sedimentary provenance analysis. *Earth Planet. Sci. Lett.* **2006**, *247*, 252–266. [[CrossRef](#)]
127. Strachan, R.A.; Prave, A.R.; Kirkland, C.L.; Storey, C.D. U-Pb detrital zircon geochronology of the Dalradian Supergroup, Shetland Islands, Scotland: Implications for regional correlations and Neoproterozoic-Palaeozoic basin development. *J. Geol. Soc.* **2013**, *170*, 905–916. [[CrossRef](#)]
128. Dhuime, B.; Bosch, D.; Bruguier, O.; Caby, R.; Pourtales, S. Age, provenance and post-deposition metamorphic overprint of detrital zircons from the Nathorst Land Group (NE Greenland)—a LA-ICP-MS and SIMS study. *Precamb. Res.* **2007**, *155*, 24–46. [[CrossRef](#)]
129. Bingen, B.; Nordgulen, Ø.; Viola, G. A four-phase model for the Sveconorwegian orogeny, SW Scandinavia. *Nor. Geol. Tidsskr.* **2008**, *88*, 43–72.
130. Chew, D.M. and Strachan, R.A. The Laurentian Caledonides of Scotland and Ireland. In *New Perspectives on the Caledonides of Scandinavia and Related Areas*; Corfu, F., Gasser, D., Chew, D.M., Eds.; Geological Society: London, UK, 2014; Special Publications; Volume 390, pp. 45–91.
131. Roberts, D.; Sturt, B.A. Caledonian deformation in Norway. *J. Geol. Soc.* **1980**, *137*, 241–250. [[CrossRef](#)]
132. Leslie, A.G.; Smith, M.; Soper, N.J. Laurentian margin evolution and the Caledonian orogeny—a template for Scotland and East Greenland. *Mem. Geol. Soc. Am.* **2008**, *202*, 307–343.
133. Lundmark, A.M.; Corfu, F. Emplacement of a Silurian granitic dyke swarm during nappe translation in the Scandinavian Caledonides. *J. Struct. Geol.* **2008**, *30*, 918–928. [[CrossRef](#)]
134. Oliver, G.J.H.; Wilde, S.A.; Wan, Y. Geochronology and geodynamics of Scottish granitoids from the Late Neoproterozoic break-up of Rodinia to Palaeozoic collision. *J. Geol. Soc.* **2008**, *165*, 661–674. [[CrossRef](#)]
135. Slagstad, T.; Davidsen, B.; Daly, J.S. Age and composition of crystalline basement rocks on the Norwegian continental margin: Offshore extension and continuity of the Caledonian-Appalachian orogenic belt. *J. Geol. Soc.* **2011**, *168*, 1167–1185. [[CrossRef](#)]
136. Pedersen, R.B.; Dunning, G.R. Evolution of arc crust and relations between contrasting sources: U-Pb (age), Nd and Sr isotope systematics of the ophiolitic terrain of SW Norway. *Contrib. Mineral. Petrol.* **1997**, *128*, 1–15. [[CrossRef](#)]
137. Kühn, A.; Glodny, J.; Austrheim, H.; Råheim, A. The Caledonian tectono-metamorphic evolution of the Lindås Nappe: Constraints from U-Pb, Sm-Nd and Rb-Sr ages of granitoid dykes. *Nor. Geol. Tidsskr.* **2002**, *82*, 45–57.
138. Andrews, S.D.; Morton, A.; Decou, A.; Frei, D. Reconstructing drainage pathways in the North Atlantic during the Triassic utilizing heavy minerals, mineral chemistry, and detrital zircon geochronology. *Geosphere* **2021**, *17*, 479–500. [[CrossRef](#)]
139. Preston, J.; Hartley, A.J.; Mange-Rajetzky, M.; Hole, M.; May, G.; Buck, S.; Vaughan, L. The provenance of Triassic continental sandstones from the Beryl Field, northern North Sea: Mineralogical, geochemical, and sedimentological constraints. *J. Sediment. Res.* **2002**, *72*, 18–29. [[CrossRef](#)]
140. Corfu, F.; Andersen, T.B. U-Pb ages of the Dalsfjord complex, SW Norway, and their bearing on the correlation of allochthonous crystalline segments of the Scandinavian Caledonides. *Int. J. Earth Sci.* **2002**, *91*, 955–963. [[CrossRef](#)]
141. Mason, A.J. The Palaeoproterozoic anatomy of the Lewisian Complex, NW Scotland: Evidence for two ‘Laxfordian’ tectonothermal cycles. *J. Geol. Soc.* **2015**, *173*, 153–169. [[CrossRef](#)]
142. Kenny, G.G.; O’Sullivan, G.J.; Alexander, S.; Simms, M.J.; Chew, D.M.; Kamber, B.S. On the track of a Scottish impact structure: A detrital zircon and apatite provenance study of the Stac Fada Member and wider Stoer Group, NW Scotland. *Geol. Mag.* **2019**, *156*, 1863–1876. [[CrossRef](#)]
143. Kirkland, C.L.; Hollis, J.; Danišić, M.; Petersen, J.; Evans, N.J.; McDonald, B.J. Apatite and titanite from the Karrat Group, Greenland; implications for charting the thermal evolution of crust from the U-Pb geochronology of common Pb bearing phases. *Precamb. Res.* **2017**, *300*, 107–120. [[CrossRef](#)]

144. Ziegler, P.A. North Sea rift system. *Tectonophysics* **1992**, *208*, 55–75. [[CrossRef](#)]
145. McKie, T. Paleogeographic evolution of latest Permian and Triassic salt basins in northwest Europe. In *Permo-Triassic Salt Provinces of Europe, North Africa and the Atlantic Margins*; Soto, J.I., Flinch, J.F., Tari, G., Eds.; Elsevier: Amsterdam, The Netherlands, 2017; pp. 159–173.

**Disclaimer/Publisher’s Note:** The statements, opinions and data contained in all publications are solely those of the individual author(s) and contributor(s) and not of MDPI and/or the editor(s). MDPI and/or the editor(s) disclaim responsibility for any injury to people or property resulting from any ideas, methods, instructions or products referred to in the content.